

Multiple Higgs models and the 125 GeV state: NMSSM and 2HDM perspectives

Jack Gunion
U.C. Davis

Particle and Astro-Particle Physics Seminar, CERN, Nov. 16, 2012

Collaborators: G. Belanger, U. Ellwanger, Y. Jiang, S. Kraml, J. Schwarz

1. *“Higgs Bosons at 98 and 125 GeV at LEP and the LHC”* G. Belanger, U. Ellwanger, J. F. Gunion, Y. Jiang, S. Kraml and J. H. Schwarz. arXiv:1210.1976 [hep-ph]
2. *“Two Higgs Bosons at the Tevatron and the LHC?”* G. Belanger, U. Ellwanger, J. F. Gunion, Y. Jiang and S. Kraml. arXiv:1208.4952 [hep-ph]
3. *“Diagnosing Degenerate Higgs Bosons at 125 GeV”* J. F. Gunion, Y. Jiang and S. Kraml. arXiv:1208.1817 [hep-ph]
4. *“Could two NMSSM Higgs bosons be present near 125 GeV?”* J. F. Gunion, Y. Jiang and S. Kraml. arXiv:1207.1545 [hep-ph]
5. *“The Constrained NMSSM and Higgs near 125 GeV”* J. F. Gunion, Y. Jiang and S. Kraml. arXiv:1201.0982 [hep-ph] Phys. Lett. B **710**, 454 (2012)

Higgs-like LHC Excesses at 125 GeV

- Experimental Higgs-like excesses: define

$$R_Y^h(X) = \frac{\sigma(pp \rightarrow Y \rightarrow h) \text{BR}(h \rightarrow X)}{\sigma(pp \rightarrow Y \rightarrow h_{SM}) \text{BR}(h_{SM} \rightarrow X)}, \quad R^h(X) = \sum_Y R_Y^h, \quad (1)$$

where $Y = gg$ or VV .

Table 1: Summary of status for 125 GeV Higgs as of HCP

$R(X)$, $X =$	$\gamma\gamma$	4ℓ	$\ell\nu\ell\nu$	$b\bar{b}$	$\tau^+\tau^-$
ATLAS	$\sim 1.8 \pm 0.5$	$\sim 1.4 \pm 0.6$	1.5 ± 0.6	$1.0 \pm 0.9 \pm 0.9 \pm 1.1$ (2012) $-0.4 \pm 0.8 \pm 0.7$ (2011+2012)	0.7 ± 0.7
CMS	$\sim 1.56 \pm 0.43$	$\sim 0.8^{+0.35}_{-0.28}$	0.74 ± 0.25	$1.3^{+0.7}_{-0.6}$	0.72 ± 0.52

In addition, we have, combining 2011 and 2012 data

$$R_{VV}^{\text{ATLAS}}(\gamma\gamma) = 2.5 \pm 1.2 \quad R_{VV}^{\text{CMS}}(\gamma\gamma) = 2.3 \pm 1.3 \quad (2)$$

and also there is the D0+CDF=Tevatron measurements of Vh production with $h \rightarrow b\bar{b}$ giving at 125 GeV

$$R_{Vh}^{\text{Tev}}(b\bar{b}) \sim 1.56 + 0.72 - 0.73. \quad (3)$$

Note: $R(ZZ, WW) \gtrsim 1$ for ATLAS, whereas $R(ZZ, WW) < 1$ for CMS.

- **The big questions:**

1. if the deviations from a single SM Higgs survive what is the model?
2. If they do survive, how far beyond our "standard" model set must we go to describe them?

Here, I focus on a number of amusing possibilities in the NMSSM and summarize some recent pure 2HDM results.

Enhanced Higgs signals in the NMSSM

- NMSSM=MSSM+ \hat{S} .
- The extra complex S component of $\hat{S} \Rightarrow$ the NMSSM has h_1, h_2, h_2, a_1, a_2 .
- The new NMSSM parameters of the superpotential (λ and κ) and scalar potential (A_λ and A_κ) appear as:

$$W \ni \lambda \hat{S} \hat{H}_u \hat{H}_d + \frac{\kappa}{3} \hat{S}^3, \quad V_{\text{soft}} \ni \lambda A_\lambda S H_u H_d + \frac{\kappa}{3} A_\kappa S^3 \quad (4)$$

- $\langle S \rangle \neq 0$ is generated by SUSY breaking and solves μ problem: $\mu_{\text{eff}} = \lambda \langle S \rangle$.
- First question: Can the NMSSM give a Higgs mass as large as 125 GeV?

Answer: Yes, so long as it is not a highly unified model. For our studies, we employed universal m_0 , except for NUHM ($m_{H_u}^2, m_{H_d}^2, m_S^2$ free), universal $A_t = A_b = A_\tau = A_0$ but allow A_λ and A_κ to vary freely. Of course, $\lambda > 0$ and κ are scanned demanding perturbativity up to the GUT scale.

- Can this model achieve rates in $\gamma\gamma$ and 4ℓ that are $> \text{SM}$?

Answer: it depends on whether or not we insist on getting good a_μ .

- The possible mechanism (arXiv:1112.3548, Ellwanger) is to reduce the $b\bar{b}$ width of the mainly SM-like Higgs by giving it some singlet component. The gg and $\gamma\gamma$ couplings are less affected.
- Typically, this requires m_{h_1} and m_{h_2} to have similar masses (for singlet-doublet mixing) and large λ (to enhance Higgs mass).

Large λ (by which we mean $\lambda > 0.1$) is only possible while retaining perturbativity up to m_{Pl} if $\tan\beta$ is modest in size.

In the semi-unified model we employ, enhanced rates and/or large λ cannot be made consistent with decent δa_μ . (J. F. Gunion, Y. Jiang and S. Kraml.arXiv:1201.0982 [hep-ph])

- The "enhanced" SM-like Higgs can be either h_1 or h_2 .

$$R_{gg}^{h_i}(X) \equiv (C_{gg}^{h_i})^2 \frac{\text{BR}(h_i \rightarrow X)}{\text{BR}(h_{SM} \rightarrow X)}, \quad R_{\text{VBF}}^{h_i}(X) \equiv (C_{\text{VV}}^{h_i})^2 \frac{\text{BR}(h_i \rightarrow X)}{\text{BR}(h_{SM} \rightarrow X)}, \quad (5)$$

where h_i is the i^{th} NMSSM scalar Higgs, and h_{SM} is the SM Higgs boson. $C_Y^{h_i} = g_{Yh_i}/g_{Yh_{SM}}$ and R_{Vh} for $V^* \rightarrow Vh_i$ ($V = W, Z$) with $h_i \rightarrow X$ is equal to $R_{\text{VBF}}^{h_i}(X)$ in doublets + singlets models.

Some illustrative R_{gg} results from (J. F. Gunion, Y. Jiang and S. Kraml. arXiv:1207.1545):

Figure Legend

	LEP/Teva	B -physics	$\Omega h^2 > 0$	$\delta a_\mu (\times 10^{10})$	XENON100	$R^{h_1/h_2}(\gamma\gamma)$
●	✓	✓	0 – 0.136	×	✓	[0.5, 1]
■	✓	✓	0 – 0.094	×	✓	(1, 1.2]
▲	✓	✓	0 – 0.094	×	✓	> 1.2
■	✓	✓	0.094-0.136	×	✓	(1, 1.2]
▲	✓	✓	0.094-0.136	×	✓	> 1.2
◆	✓	✓	0.094 – 0.136	4.27-49.1	✓	~ 1

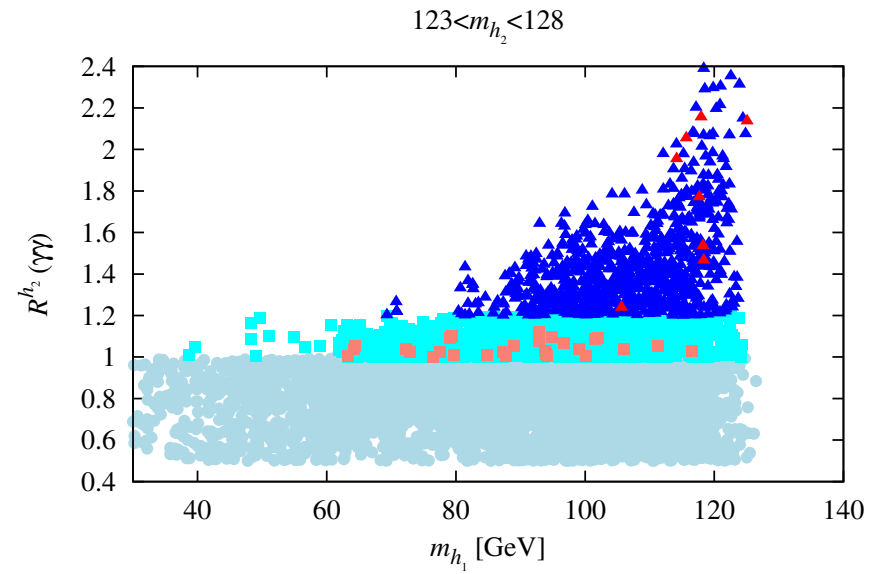
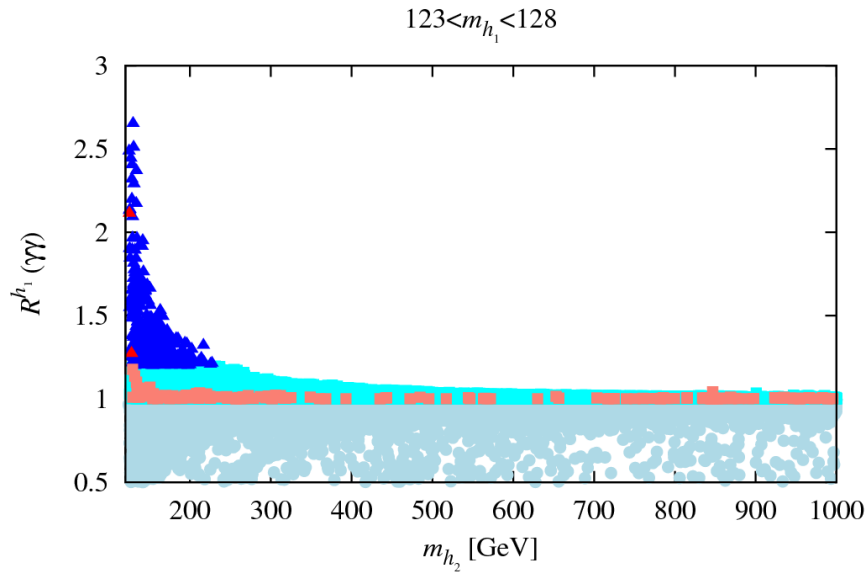


Figure 1: The plot shows $R_{gg}(\gamma\gamma)$ for the cases of $123 < m_{h_1} < 128$ GeV and $123 < m_{h_2} < 128$ GeV. Note: **red triangle** (**orange square**) is for WMAP window with $R_{gg}(\gamma\gamma) > 1.2$ ($R_{gg}(\gamma\gamma) = [1, 1.2]$).

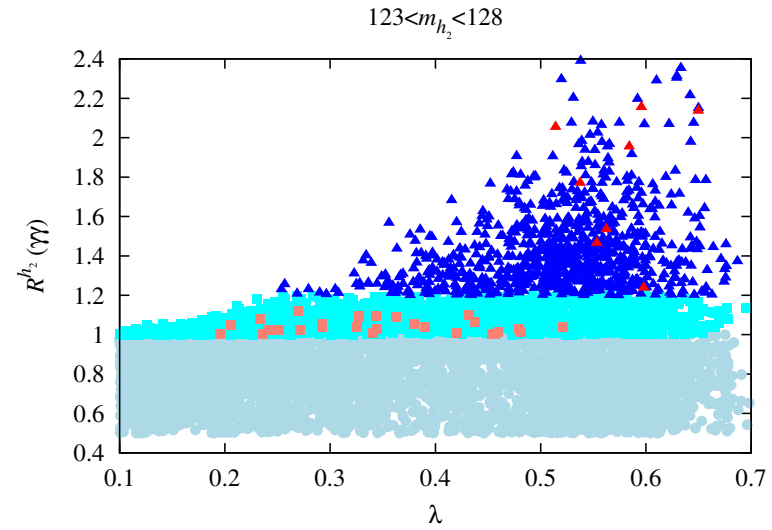
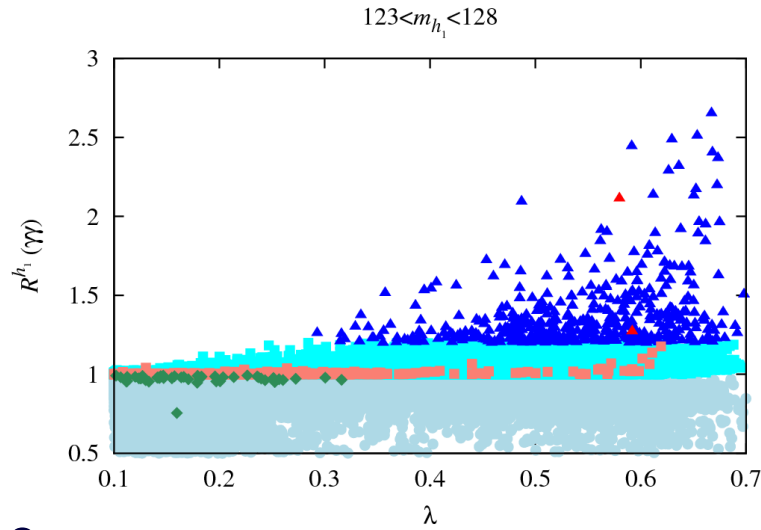


Figure 2: Observe the clear general increase in maximum $R_{gg}(\gamma\gamma)$ with increasing λ . Green points have good δa_μ , $m_{h_2} > 1$ TeV **BUT** $R_{gg}(\gamma\gamma) \sim 1$.

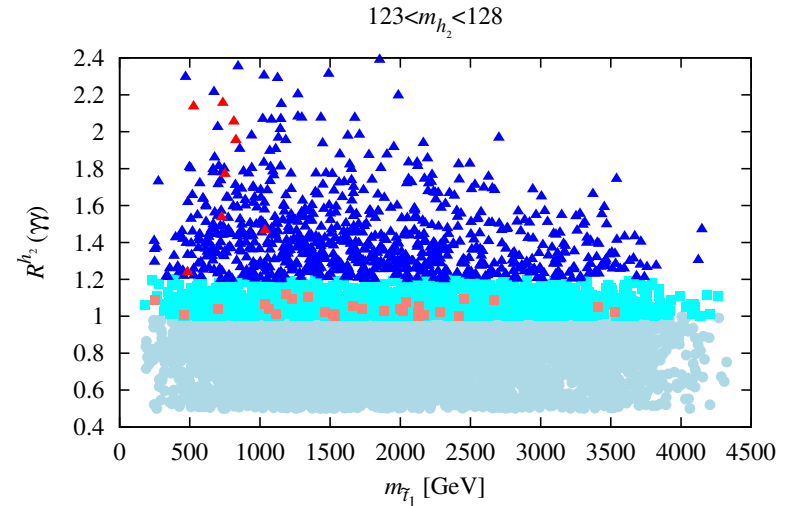
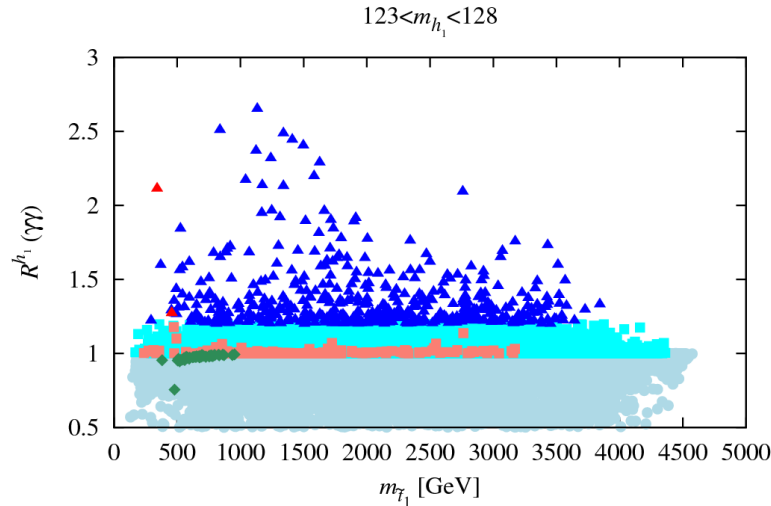


Figure 3: The lightest stop has mass $\sim 300 - 700$ GeV for red-triangle points.

- If we ignore δa_μ , then $R_{gg}(\gamma\gamma) > 1.2$ (even > 2) is possible while satisfying all other constraints provided h_1 and h_2 are close in mass, especially in the case where $m_{h_2} \in [123, 128]$ GeV window.
- This raises the issue of scenarios in which *both* m_{h_1} and m_{h_2} are in the $[123, 128]$ GeV window where the experiments see the Higgs signal.
- If h_1 and h_2 are sufficiently degenerate, the experimentalists might not have resolved the two distinct peaks, even in the $\gamma\gamma$ channel.
- The rates for the h_1 and h_2 could then add together to give an enhanced $\gamma\gamma$, for example, signal.
- The apparent width or shape of the $\gamma\gamma$ mass distribution could be altered.
- There is more room for an apparent mismatch between the $\gamma\gamma$ channel and other channels, such as $b\bar{b}$ or 4ℓ , than in non-degenerate situation.

In particular, the h_1 and h_2 will generally have different gg and VV production rates and branching ratios.

Degenerate NMSSM Higgs Scenarios:

(arXiv:1207.1545, JFG, Jiang, Kraml)

- For the numerical analysis, we use NMSSMTools version 3.2.0, which has improved convergence of RGEs in the case of large Yukawa couplings.
- The precise constraints imposed are the following.
 1. Basic constraints: proper RGE solution, no Landau pole, neutralino LSP, Higgs and SUSY mass limits as implemented in NMSSMTools-3.2.0.
 2. B physics: $\text{BR}(B_s \rightarrow X_s \gamma)$, ΔM_s , ΔM_d , $\text{BR}(B_s \rightarrow \mu^+ \mu^-)$ (old upper limit), $\text{BR}(B^+ \rightarrow \tau^+ \nu_\tau)$ and $\text{BR}(B \rightarrow X_s \mu^+ \mu^-)$ at 2σ as encoded in NMSSMTools-3.2.0, plus updates.
 3. Dark Matter: $\Omega h^2 < 0.136$, thus allowing for scenarios in which the relic density arises at least in part from some other source.
However, we single out points with $0.094 \leq \Omega h^2 \leq 0.136$, which is the ‘WMAP window’ defined in NMSSMTools-3.2.0.

4. 2011 XENON 100: spin-independent LSP–proton scattering cross section bounds implied by the neutralino-mass-dependent XENON100 bound. (For points with $\Omega h^2 < 0.094$, we rescale these bounds by a factor of $0.11/\Omega h^2$.) (2012 XENON 100 has little additional impact.)
5. δa_μ ignored: impossible to satisfy for scenarios we study here.

- Compute the effective Higgs mass in given production and final decay channels Y and X , respectively, and R_{gg}^h as

$$m_h^Y(X) \equiv \frac{R_Y^{h_1}(X)m_{h_1} + R_Y^{h_2}(X)m_{h_2}}{R_Y^{h_1}(X) + R_Y^{h_2}(X)} \quad R_Y^h(X) = R_Y^{h_1}(X) + R_Y^{h_2}(X). \quad (6)$$

- The extent to which it is appropriate to combine the rates from the h_1 and h_2 depends upon the degree of degeneracy and the experimental resolution.

Very roughly, one should probably think of $\sigma_{\text{res}} \sim 1.5$ GeV or larger. **The widths of the h_1 and h_2 are very much smaller than this resolution.**

- We perform scans covering the following parameter ranges:

$$0 \leq m_0 \leq 3000; \quad 100 \leq m_{1/2} \leq 3000; \quad 1 \leq \tan \beta \leq 40;$$

$$\begin{aligned} -6000 \leq A_0 \leq 6000; & 0.1 \leq \lambda \leq 0.7; & 0.05 \leq \kappa \leq 0.5; \\ -1000 \leq A_\lambda \leq 1000; & -1000 \leq A_\kappa \leq 1000; & 100 \leq \mu_{eff} \leq 500. \end{aligned} \quad (7)$$

We only display points which pass the basic constraints, satisfy *B*-physics constraints, have $\Omega h^2 < 0.136$, obey the 2011 XENON100 limit on the LSP scattering cross-section off protons *and* have *both* h_1 and h_2 in the desired mass range: $123 \text{ GeV} < m_{h_1}, m_{h_2} < 128 \text{ GeV}$.

- In Fig. 4, points are color coded according to $m_{h_2} - m_{h_1}$.

Circular points have $\Omega h^2 < 0.094$, while diamond points have $0.094 \leq \Omega h^2 \leq 0.136$ (*i.e.* lie within the WMAP window).

- Many of the displayed points are such that $R_{gg}^{h_1}(\gamma\gamma) + R_{gg}^{h_2}(\gamma\gamma) > 1$.
- A few such points have Ωh^2 in the WMAP window.

These points are such that either $R_{gg}^{h_1}(\gamma\gamma) > 2$ or $R_{gg}^{h_2}(\gamma\gamma) > 2$, with the $R_{gg}^h(\gamma\gamma)$ for the other Higgs being small.

- However, the majority of the points with $R_{gg}^{h_1}(\gamma\gamma) + R_{gg}^{h_2}(\gamma\gamma) > 1$ have $\Omega h^2 < 0.094$ and the $\gamma\gamma$ signal is often shared between the h_1 and the h_2 .

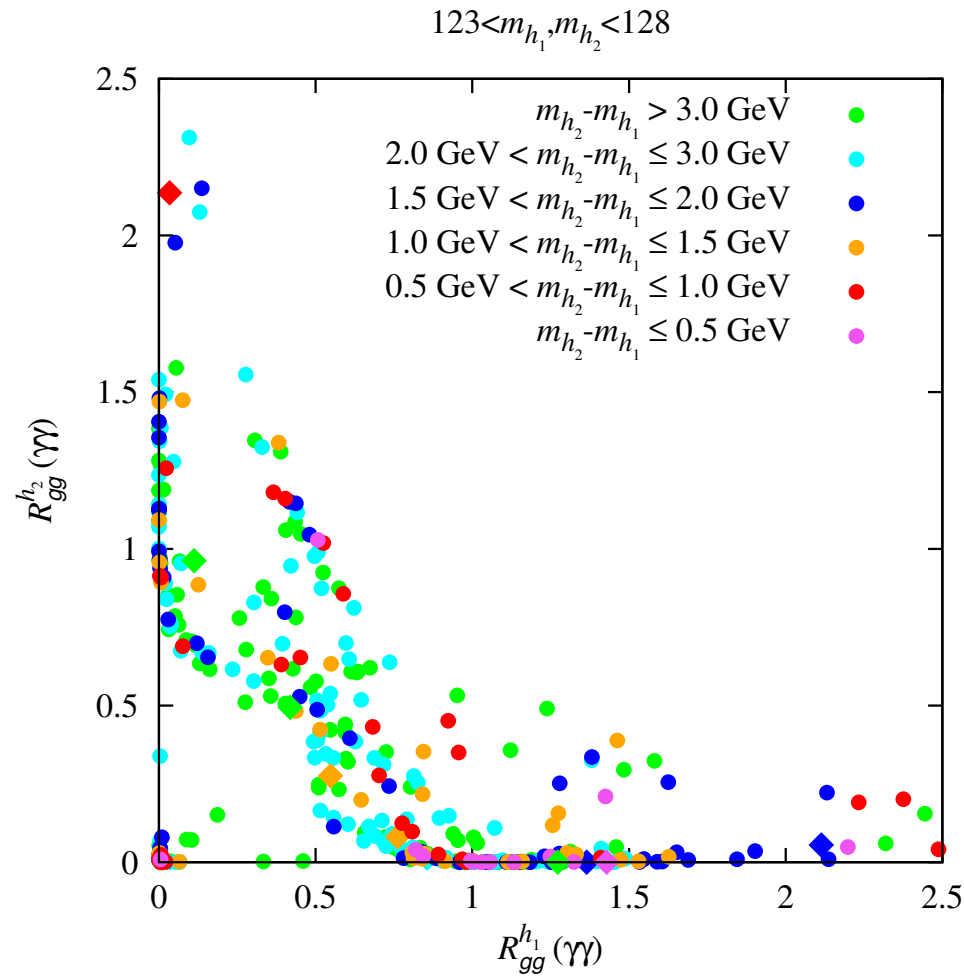


Figure 4: Correlation of $gg \rightarrow (h_1, h_2) \rightarrow \gamma\gamma$ signal strengths when both h_1 and h_2 lie in the 123–128 GeV mass range. The circular points have $\Omega h^2 < 0.094$, while diamond points have $0.094 \leq \Omega h^2 \leq 0.136$. Points are color coded according to $m_{h_2} - m_{h_1}$. Probably green and cyan points can be resolved in mass.

Now combine the h_1 and h_2 signals as described above. Recall: circular (diamond) points have $\Omega h^2 < 0.094$ ($0.094 \leq \Omega h^2 \leq 0.136$). Color code:

1. **red** for $m_{h_2} - m_{h_1} \leq 1$ GeV;
 2. **blue** for $1 \text{ GeV} < m_{h_2} - m_{h_1} \leq 2$ GeV;
 3. **green** for $2 \text{ GeV} < m_{h_2} - m_{h_1} \leq 3$ GeV.
- For current statistics and $\sigma_{\text{res}} \gtrsim 1.5$ GeV we estimate that the h_1 and h_2 signals will not be seen separately for $m_{h_2} - m_{h_1} \leq 2$ GeV.
 - In Fig. 5, we show results for $R_{gg}^h(X)$ for $X = \gamma\gamma, VV, b\bar{b}$. Enhanced $\gamma\gamma$ and VV rates from gluon fusion are very common.
 - The bottom-right plot shows that enhancement in the Vh with $h \rightarrow b\bar{b}$ rate is also natural, though not as large as the best fit value suggested by the new Tevatron analysis.
 - Diamond points (*i.e.* those in the WMAP window) are rare, but typically show enhanced rates.

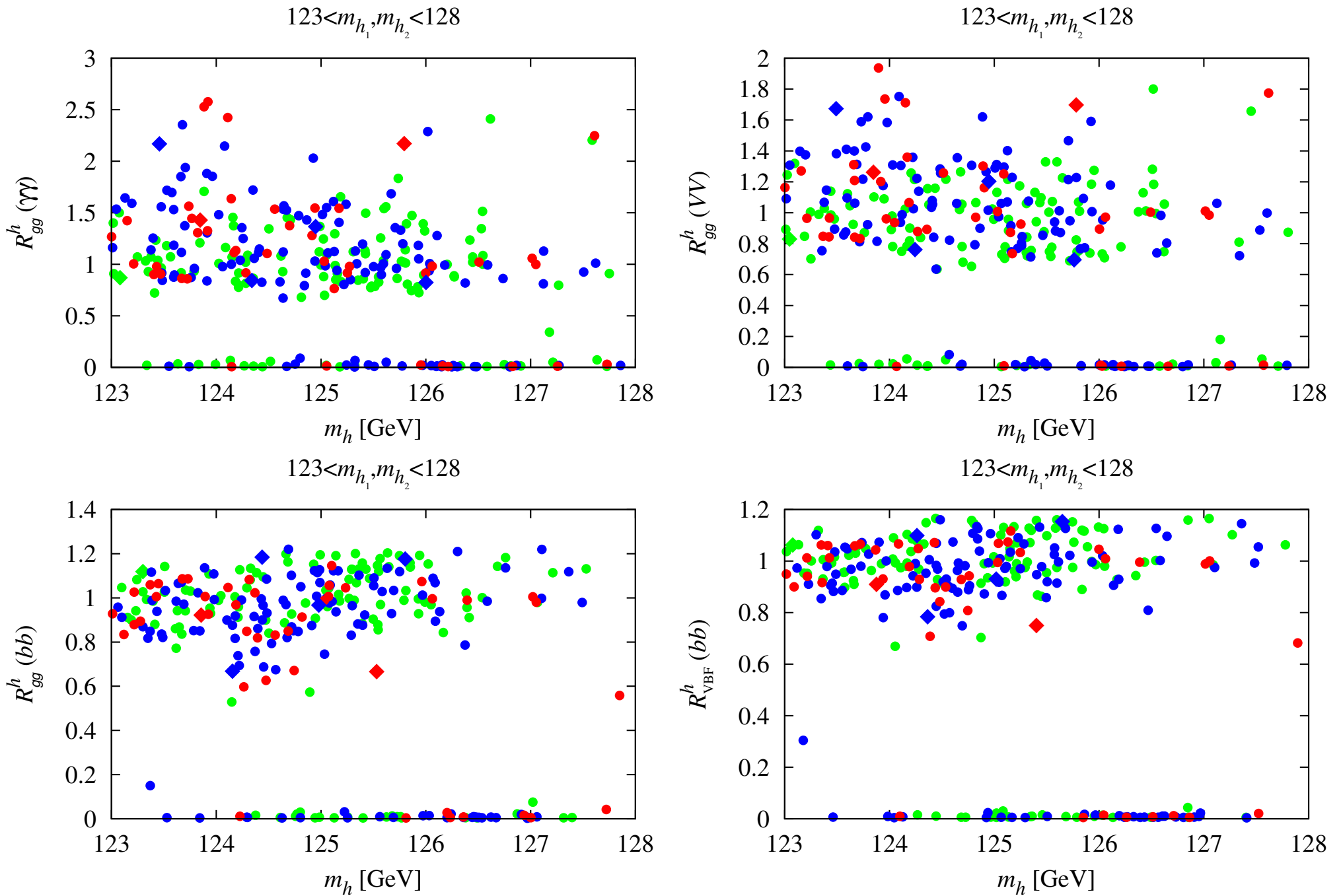


Figure 5: $R_{gg}^h(X)$ for $X = \gamma\gamma, VV, b\bar{b}$, and $R_{\text{VBF}}^h(b\bar{b})$ versus m_h . For application to the Tevatron, note that $R_{\text{VBF}}^h(b\bar{b}) = R_{V^* \rightarrow Vh}^h(b\bar{b})$.

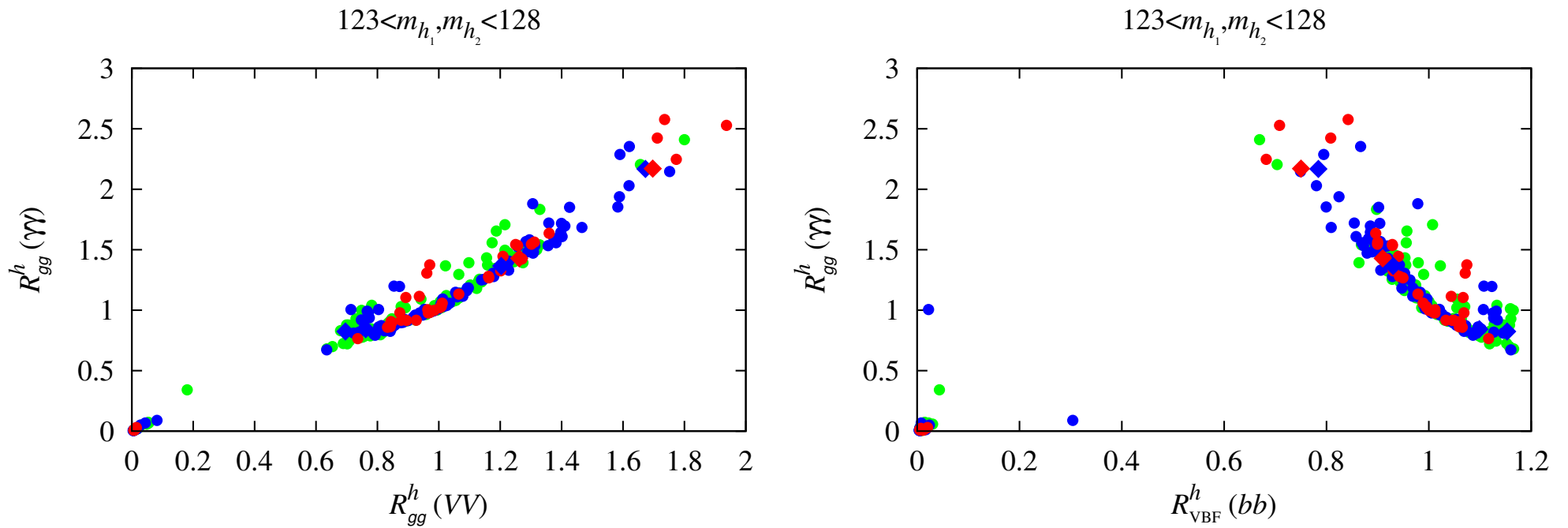


Figure 6: Left: correlation between the gluon fusion induced $\gamma\gamma$ and VV rates relative to the SM. Right: correlation between the gluon fusion induced $\gamma\gamma$ rate and the VV fusion induced $b\bar{b}$ rates relative to the SM; the relative rate for $V^* \rightarrow Vh$ with $h \rightarrow b\bar{b}$ (relevant for the Tevatron) is equal to the latter.

- **Comments on Fig. 6:**

1. Left-hand plot shows the strong correlation between $R_{gg}^h(\gamma\gamma)$ and $R_{gg}^h(VV)$.

Note that if $R_{gg}^h(\gamma\gamma) \sim 1.5$, as suggested by current experimental results, then in this model $R_{gg}^h(VV) \geq 1.2$.

2. The right-hand plot shows the (anti) correlation between $R_{gg}^h(\gamma\gamma)$ and $R_{V^* \rightarrow Vh}^h(b\bar{b}) = R_{VBF}^h(b\bar{b})$.

In general, the larger $R_{gg}^h(\gamma\gamma)$ is, the smaller the value of $R_{V^* \rightarrow Vh}^h(b\bar{b})$.

However, this latter plot shows that there *are* parameter choices for which both the $\gamma\gamma$ rate at the LHC and the $V^* \rightarrow Vh(\rightarrow b\bar{b})$ rate at the Tevatron (and LHC) can be enhanced relative to the SM as a result of there being contributions to these rates from both the h_1 and h_2 .

3. It is often the case that one of the h_1 or h_2 dominates $R_{gg}^h(\gamma\gamma)$ while the other dominates $R_{V^* \rightarrow Vh}^h(b\bar{b})$. This is typical of the diamond WMAP-window points.

However, a significant number of the circular $\Omega h^2 < 0.094$ points are such that either the $\gamma\gamma$ or the $b\bar{b}$ signal receives substantial contributions from both the h_1 and the h_2 .

We did not find points where the $\gamma\gamma$ and $b\bar{b}$ final states *both* receive substantial contributions from *both* the h_1 and h_2 .

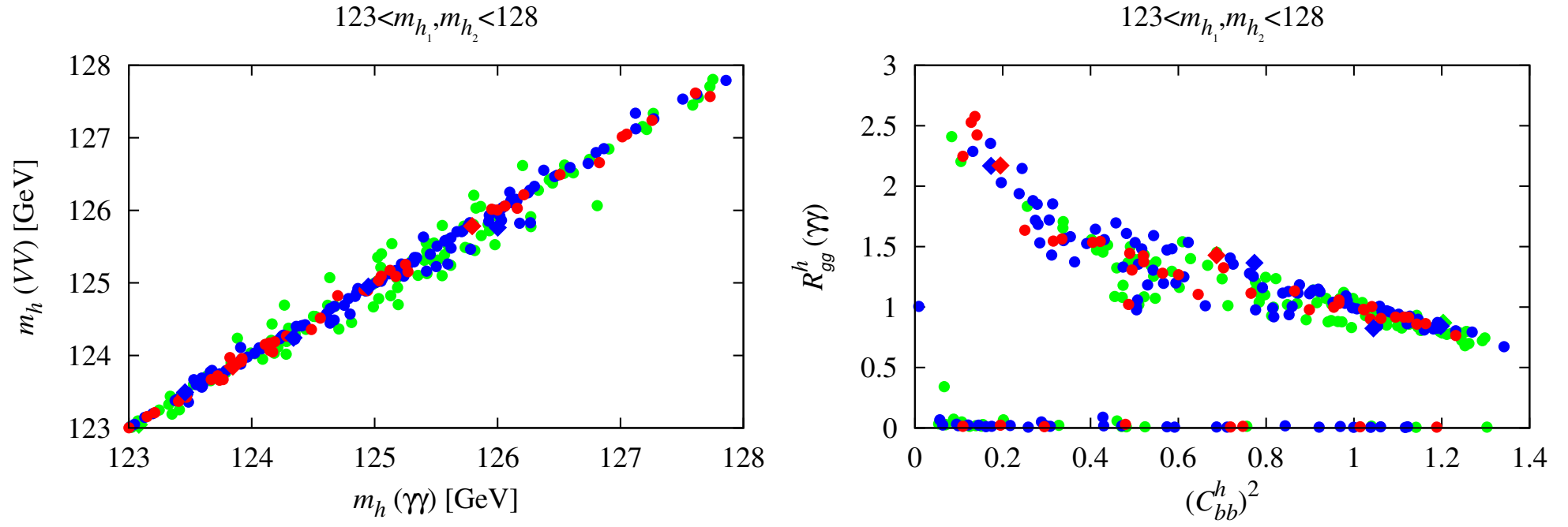


Figure 7: Left: effective Higgs masses obtained from different channels: $m_h^{gg}(\gamma\gamma)$ versus $m_h^{gg}(VV)$. Right: $\gamma\gamma$ signal strength $R_{gg}^h(\gamma\gamma)$ versus effective coupling to $b\bar{b}$ quarks $(C_{bb}^h)^2$. Here, $C_{bb}^h \equiv [R_{gg}^{h1}(\gamma\gamma)C_{bb}^{h1} + R_{gg}^{h2}(\gamma\gamma)C_{bb}^{h2}] / [R_{gg}^{h1}(\gamma\gamma) + R_{gg}^{h2}(\gamma\gamma)]$.

Comments on Fig. 7

1. The m_h values for the gluon fusion induced $\gamma\gamma$ and VV cases are also strongly correlated — in fact, they differ by no more than a fraction of a

GeV and are most often much closer, see the left plot of Fig. 7.

2. The right plot of Fig. 7 illustrates the mechanism behind enhanced rates, namely that large net $\gamma\gamma$ branching ratio is achieved by reducing the average total width by reducing the average $b\bar{b}$ coupling strength.

- The dependence of $R_{gg}^h(\gamma\gamma)$ on λ , κ , $\tan\beta$ and μ_{eff} is illustrated in Fig. 8.

We observe that the largest $R_{gg}^h(\gamma\gamma)$ values arise at large λ , moderate κ , small $\tan\beta < 5$ (but note that $R_{gg}^h(\gamma\gamma) > 1.5$ is possible even for $\tan\beta = 15$) and small $\mu_{\text{eff}} < 150$ GeV.

Such low values of μ_{eff} are very favorable in point of view of fine-tuning, in particular if stops are also light.

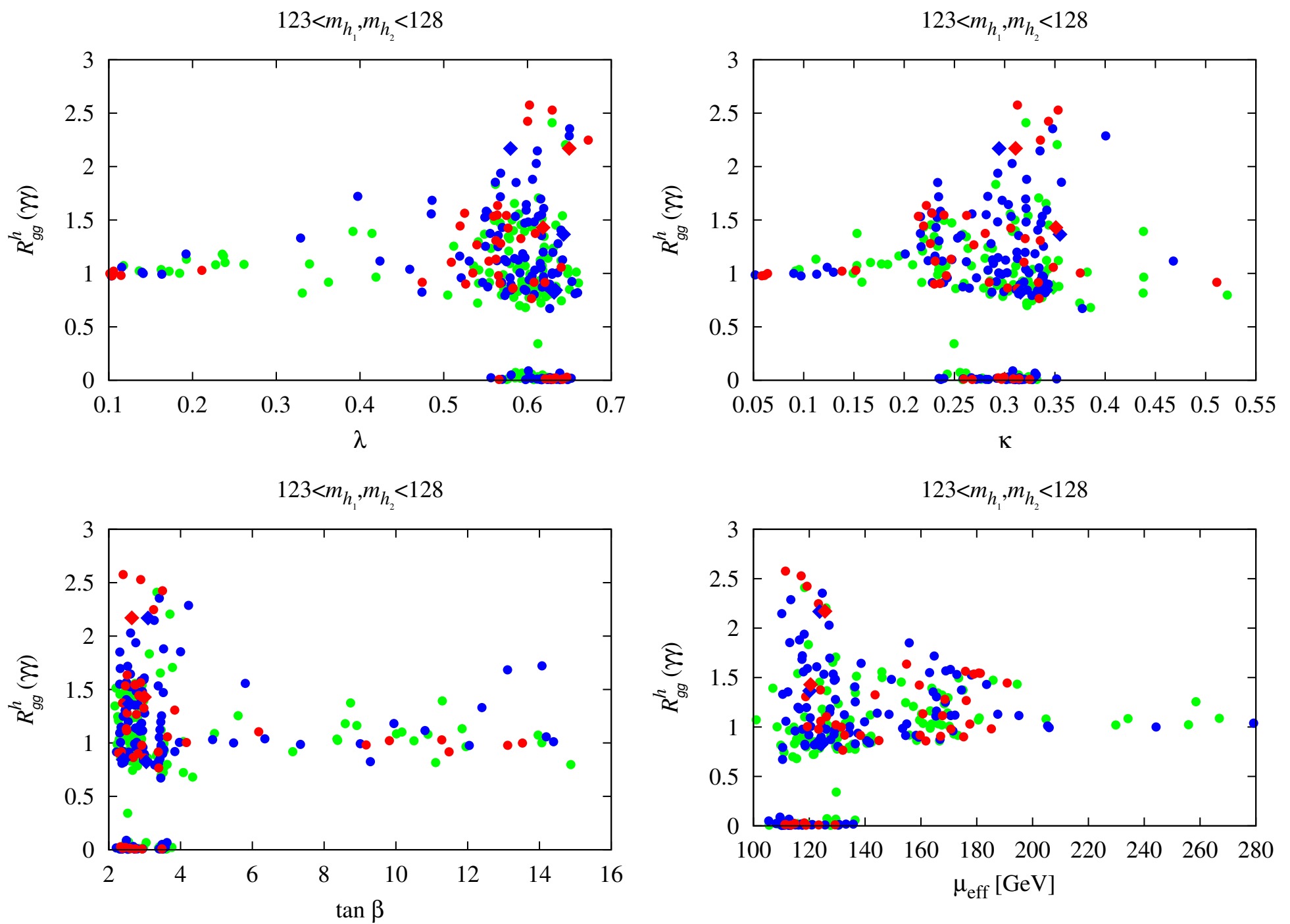


Figure 8: Dependence of $R_{gg}^h(\gamma\gamma)$ on λ , κ , $\tan \beta$ and μ_{eff} .

Fig. 9 shows that the stop mixing is typically large in these cases, $(A_t - \mu_{\text{eff}} \cot \beta)/M_{\text{SUSY}} \approx 1.5\text{--}2$. Moreover, the few points which we found in the WMAP window always have $m_{\tilde{t}_1} < 700$ GeV.

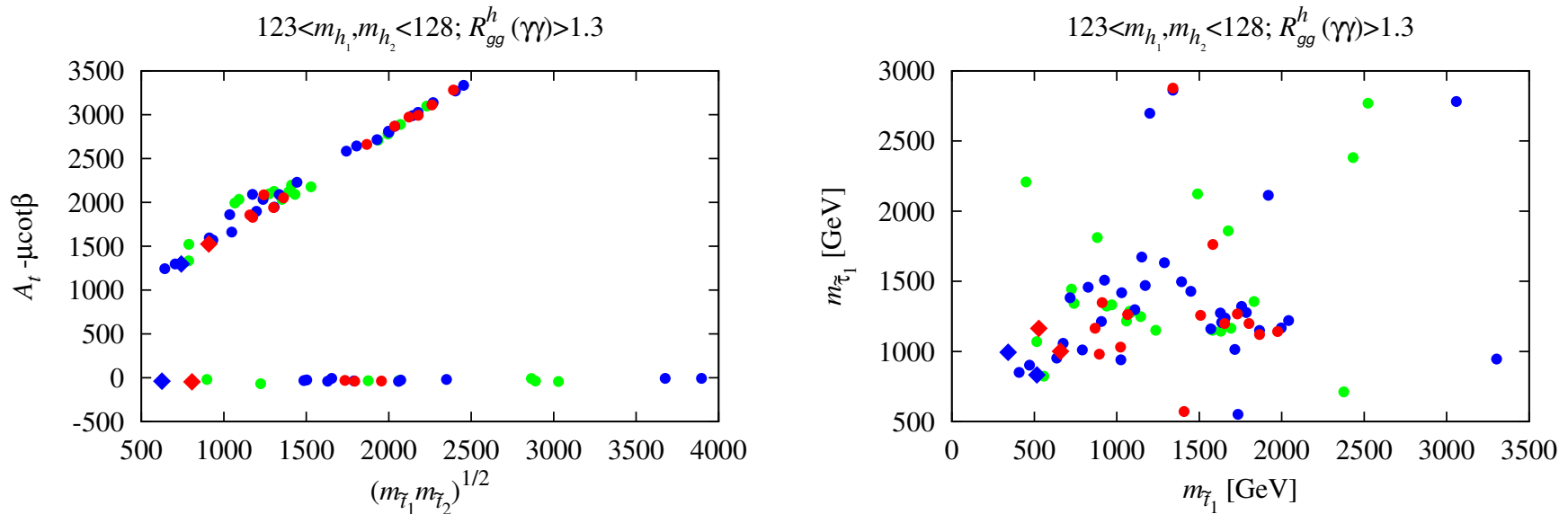


Figure 9: Left: Stop mixing parameter vs. $M_{\text{SUSY}} \equiv \sqrt{m_{\tilde{t}_1} m_{\tilde{t}_2}}$. Right: $m_{\tilde{\tau}_1}$ vs. $m_{\tilde{\tau}_1}$. Points plotted have $R_{gg}^h(\gamma\gamma) > 1.3$.

- Implications of the enhanced $\gamma\gamma$ rate scenarios for other observables are also quite interesting.

First, let us observe from Fig. 10 that these scenarios have squark and gluino masses that are above about 1.25 TeV ranging up to as high as 6 TeV (where our scanning more or less ended).

The WMAP-window points with large $R_{gg}^h(\gamma\gamma)$ are located at low masses of $m_{\tilde{g}} \sim 1.3$ TeV and $m_{\tilde{q}} \sim 1.6$ TeV.

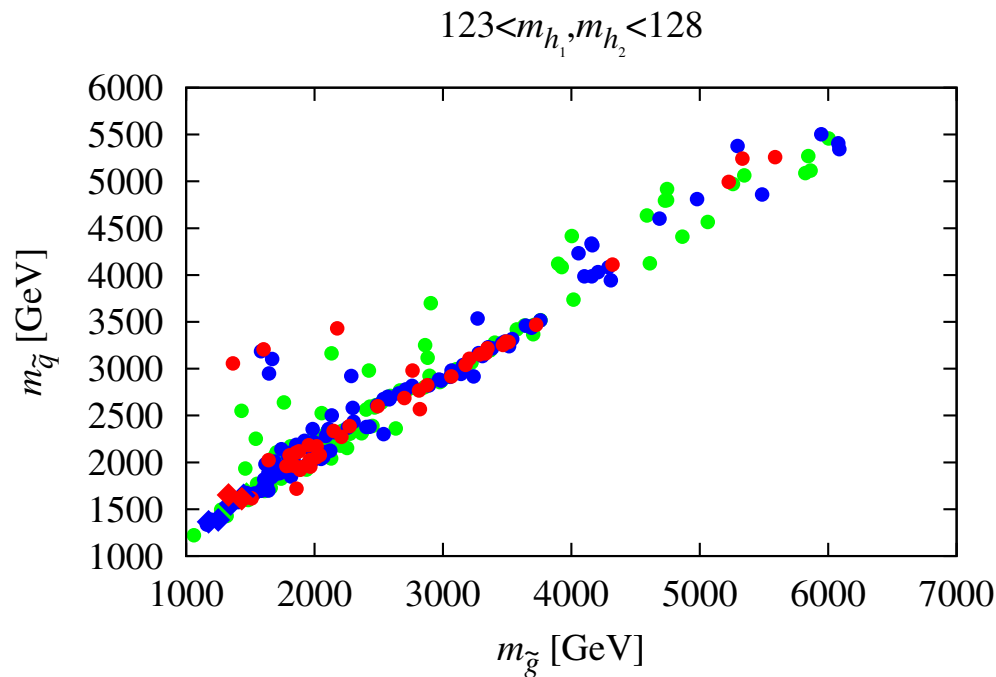


Figure 10: Average light-flavor squark mass, $m_{\tilde{q}}$, versus gluino mass, $m_{\tilde{g}}$, for the points plotted in the previous figures.

- The value of $R_{gg}^h(\gamma\gamma)$ as a function of the masses of the other Higgs bosons is illustrated in Fig. 11.

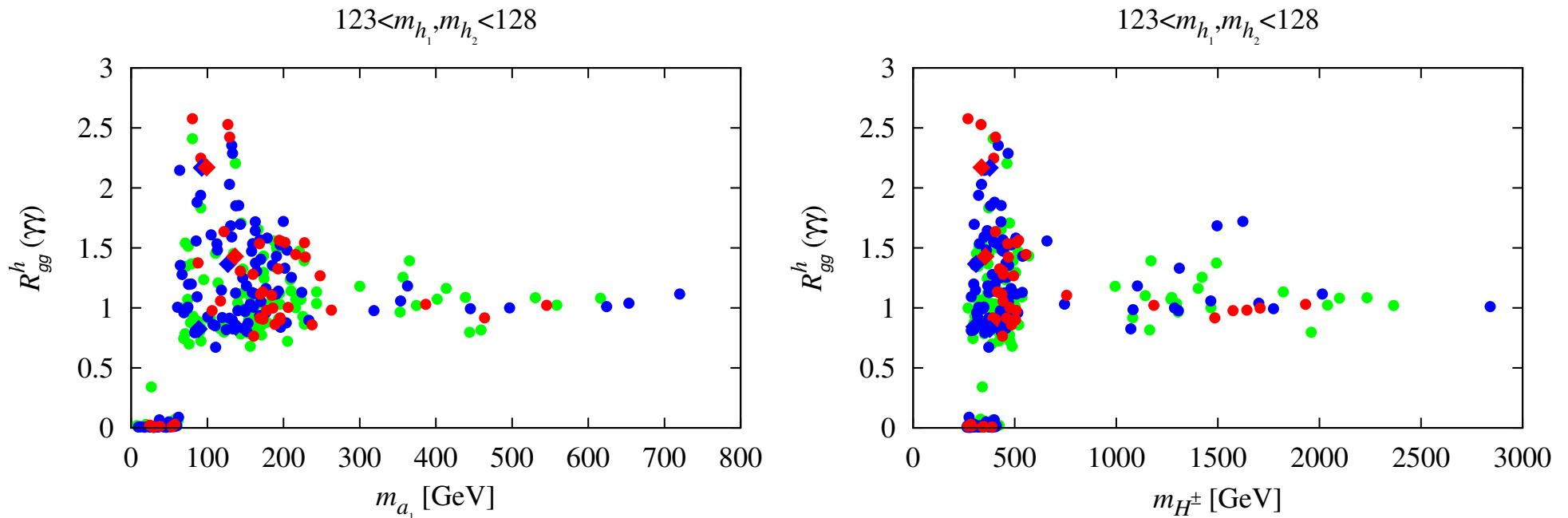


Figure 11: $R_{gg}^h(\gamma\gamma)$ versus the masses of m_{a_1} and m_{H^\pm} (note that $m_{H^\pm} \simeq m_{a_2} \simeq m_{h_3}$).

Comments on Fig. 11:

1. We see that values above of $R^h(\gamma\gamma) > 1.7$ are associated with masses

for the a_2 , h_3 and H^\pm of order $\lesssim 500$ GeV and for the a_1 of order $\lesssim 150$ GeV.

(Note that $m_{a_2} \simeq m_{h_3} \simeq m_{H^\pm}$)

Although these states have moderate masses, their detectability requires further study.

2. One interesting point is that $m_{a_1} \sim 125$ GeV is common for points with $R_{gg}^h(\gamma\gamma) > 1$ points.

We have checked that $R_{gg}^{a_1}(\gamma\gamma)$ is quite small for such points — typically $\lesssim 0.01$.

- In Fig. 12, we display Ωh^2 and the spin-independent cross section for LSP scattering on protons, σ_{SI} , for the points plotted in previous figures.

Comments on Fig. 12:

1. Very limited range of LSP masses consistent with the WMAP window, roughly $m_{\tilde{\chi}_1^0} \in [60, 80]$ GeV.
2. Corresponding σ_{SI} values range from $few \times 10^{-9}$ pb to as low as $few \times 10^{-11}$ pb.

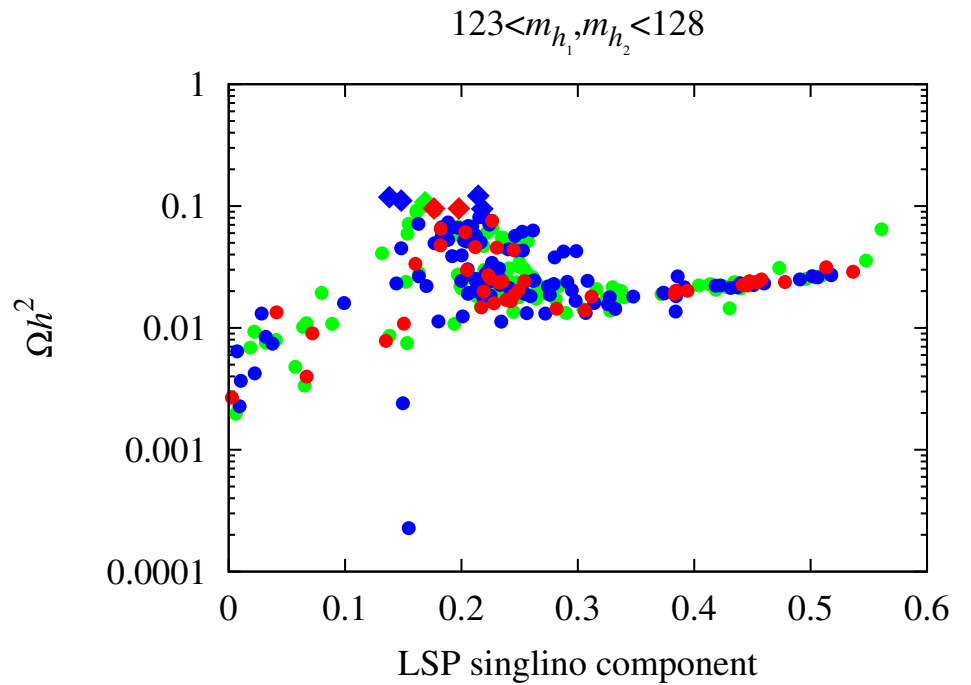
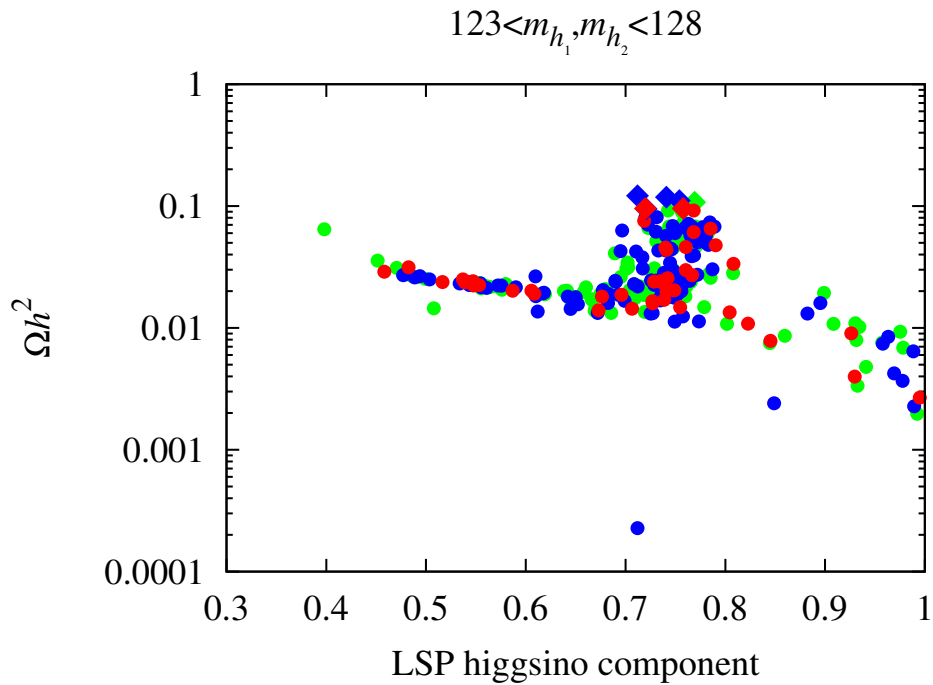
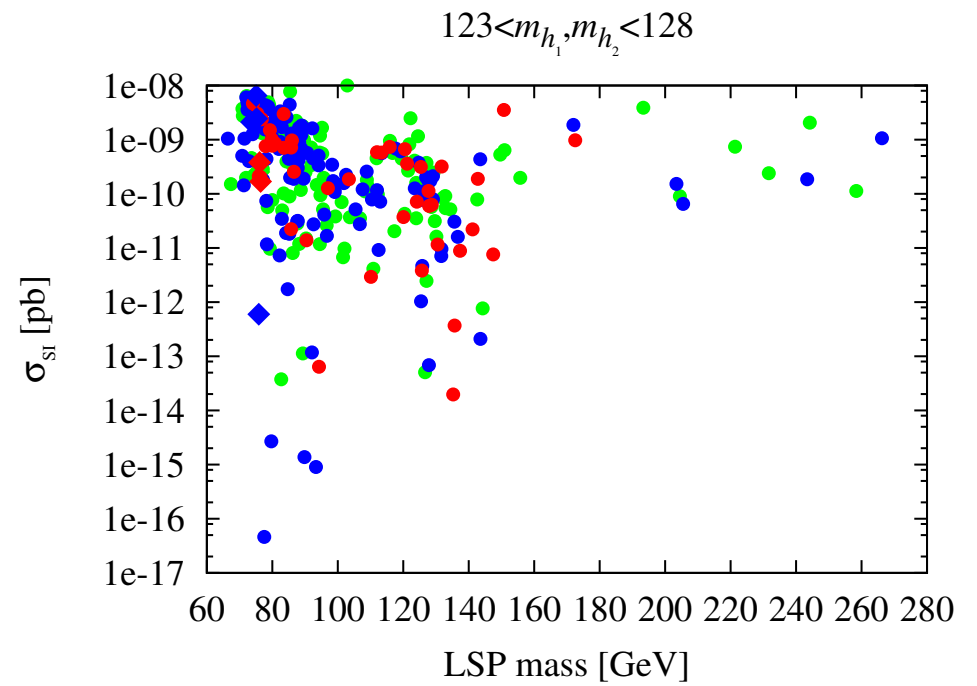
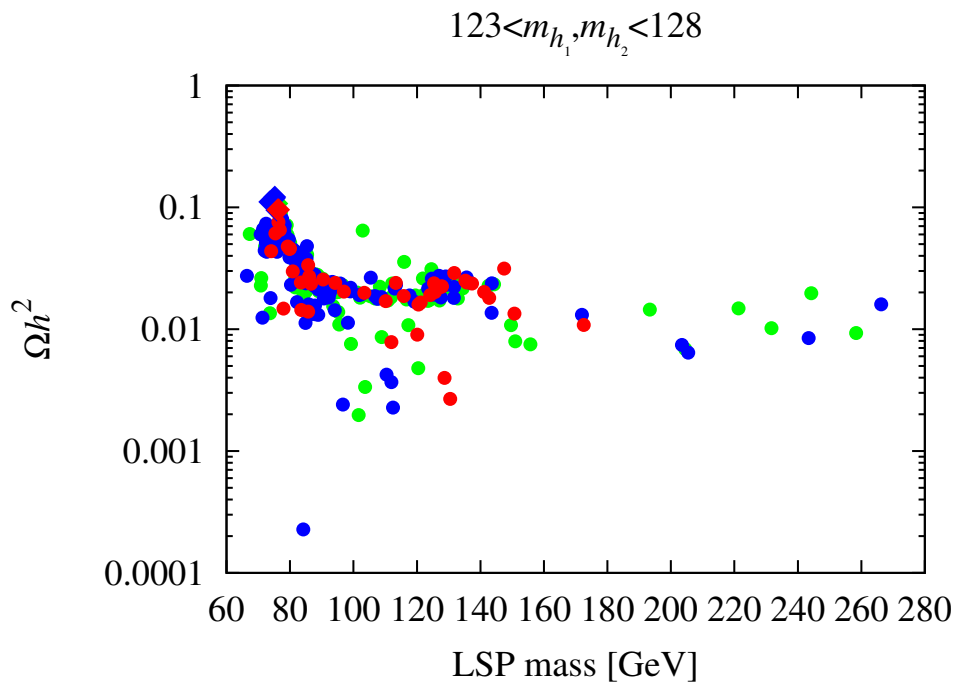


Figure 12: Top row: Ωh^2 and spin-independent cross section on protons versus LSP mass for the points plotted in previous figures. Bottom row: Ωh^2 versus LSP higgsino (left) and singlino (right) components.

3. Owing to the small μ_{eff} , the LSP is dominantly higgsino, which is also the reason for Ωh^2 typically being too low.

The points with Ωh^2 within the WMAP window are mixed higgsino–singlino, with a singlino component of the order of 20%, see the bottom-row plots of Fig. 12.

- It is interesting to note a few points regarding the parameters associated with the points plotted in previous figures.
 1. For the WMAP-window diamond points, $\lambda \in [0.58, 0.65]$, $\kappa \in [0.28, 0.35]$, and $\tan \beta \in [2.5, 3.5]$.
 2. Points with $R_{gg}^h(\gamma\gamma) > 1.3$ have $\lambda \in [0.33, 0.67]$, $\kappa \in [0.22, 0.36]$, and $\tan \beta \in [2, 14]$.
- Can't find scenarios of this degenerate/enhanced type such that δa_μ is consistent with that needed to explain the current discrepancy.

In particular, the very largest value of δa_μ achieved is of order 1.8×10^{-10} and, further, the WMAP-window points with large $R_{gg}^h(\gamma\gamma, VV)$ have $\delta a_\mu < 6 \times 10^{-11}$.

Diagnosing the presence of degenerate Higgses

(J. F. Gunion, Y. Jiang and S. Kraml. arXiv:1208.1817)

- Given that enhanced R_{gg}^h is very natural if there are degenerate Higgs mass eigenstates, **how do we detect degeneracy?** Must look at correlations among different R^h 's.
- In the context of any doublets plus singlets model not all the R^{h_i} 's are independent; a complete independent set of R^h 's can be taken to be:

$$R_{gg}^h(VV), \quad R_{gg}^h(bb), \quad R_{gg}^h(\gamma\gamma), \quad R_{VBF}^h(VV), \quad R_{VBF}^h(bb), \quad R_{VBF}^h(\gamma\gamma). \quad (8)$$

Let us now look in more detail at a given $R_Y^h(X)$. It takes the form

$$R_Y^h(X) = \sum_{i=1,2} \frac{(C_Y^{h_i})^2 (C_X^{h_i})^2}{C_\Gamma^{h_i}} \quad (9)$$

where $C_X^{h_i}$ for $X = \gamma\gamma, WW, ZZ, \dots$ is the ratio of the $h_i X$ to $h_{SM} X$ coupling and $C_\Gamma^{h_i}$ is the ratio of the total width of the h_i to the SM Higgs

total width. The diagnostic tools that can reveal the existence of a second, quasi-degenerate (but non-interfering in the small width approximation) Higgs state are the double ratios:

$$\text{I): } \frac{R_{VBF}^h(\gamma\gamma)/R_{gg}^h(\gamma\gamma)}{R_{VBF}^h(bb)/R_{gg}^h(bb)}, \quad \text{II): } \frac{R_{VBF}^h(\gamma\gamma)/R_{gg}^h(\gamma\gamma)}{R_{VBF}^h(VV)/R_{gg}^h(VV)}, \quad \text{III): } \frac{R_{VBF}^h(VV)/R_{gg}^h(VV)}{R_{VBF}^h(bb)/R_{gg}^h(bb)}, \quad (10)$$

each of which should be unity if only a single Higgs boson is present but, due to the non-factorizing nature of the sum in Eq. (9), are generally expected to deviate from 1 if two (or more) Higgs bosons are contributing to the net h signals.

In a doublets+singlets model all other double ratios that are equal to unity for single Higgs exchange are not independent of the above three.

Of course, the above three double ratios are not all independent.

Which will be most useful depends upon the precision with which the R^h 's for different initial/final states can be measured.

E.g measurements of R^h for the bb final state may continue to be somewhat imprecise and it is then double ratio II) that might prove most discriminating.

Or, it could be that one of the double ratios deviates from unity by a much larger amount than the others, in which case it might be most discriminating even if the R^h 's involved are not measured with great precision.

- In Fig. 13, we plot the numerator versus the denominator of the double ratios I) and II), [III) being very like I) due to the correlation between the $R_{gg}^h(\gamma\gamma)$ and $R_{gg}^h(VV)$ values discussed earlier].
- We observe that any one of these double ratios will often, but not always, deviate from unity (the diagonal dashed line in the figure).
- The probability of such deviation increases dramatically if we require (as apparently preferred by LHC data) $R_{gg}^h(\gamma\gamma) > 1$, see the solid (vs. open) symbols of Fig. 13.

This is further elucidated in Fig. 14 where we display the double ratios I) and II) as functions of $R_{gg}^h(\gamma\gamma)$ (left plots).

For the NMSSM, it seems that the double ratio I) provides the greatest discrimination between degenerate vs. non-degenerate scenarios with values

very substantially different from unity (the dashed line) for the majority of the degenerate NMSSM scenarios explored in the earlier section of this talk that have enhanced $\gamma\gamma$ rates.

Note in particular that I), being sensitive to the $b\bar{b}$ final state, singles out degenerate Higgs scenarios even when one or the other of h_1 or h_2 dominates the $gg \rightarrow \gamma\gamma$ rate, see the top right plot of Fig. 14.

In comparison, double ratio II) is most useful for scenarios with $R_{gg}^h(\gamma\gamma) \sim 1$, as illustrated by the bottom left plot of Fig. 14.

- Thus, as illustrated by the bottom right plot of Fig. 14, the greatest discriminating power is clearly obtained by measuring both double ratios.

In fact, a close examination reveals that there are no points for which *both* double ratios are exactly 1!

Of course, experimental errors may lead to a region containing a certain number of points in which both double ratios are merely consistent with 1 within the errors.

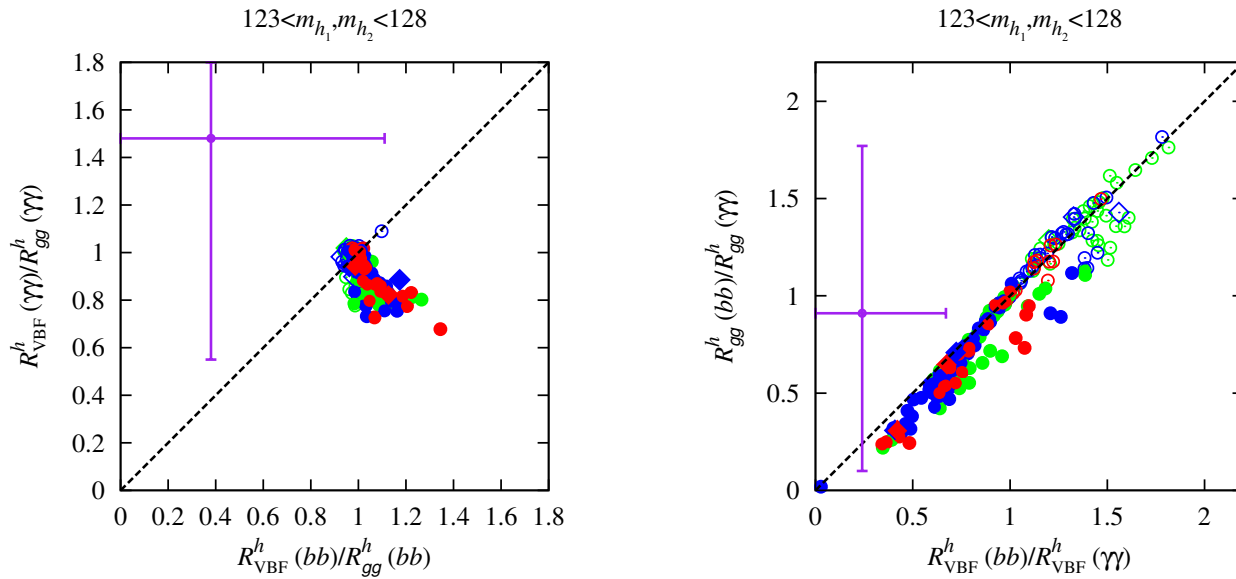


Figure 13: Comparisons of pairs of event rate ratios that should be equal if only a single Higgs boson is present. The color code is green for points with $2 \text{ GeV} < m_{h_2} - m_{h_1} \leq 3 \text{ GeV}$, blue for $1 \text{ GeV} < m_{h_2} - m_{h_1} \leq 2 \text{ GeV}$, and red for $m_{h_2} - m_{h_1} \leq 1 \text{ GeV}$. Large diamond points have Ωh^2 in the WMAP window of $[0.094, 0.136]$, while circular points have $\Omega h^2 < 0.094$. Solid points are those with $R_{\text{gg}}^h(\gamma\gamma) > 1$ and open symbols have $R_{\text{gg}}^h(\gamma\gamma) \leq 1$. Current experimental values for the ratios from CMS data along with their 1σ error bars are also shown.

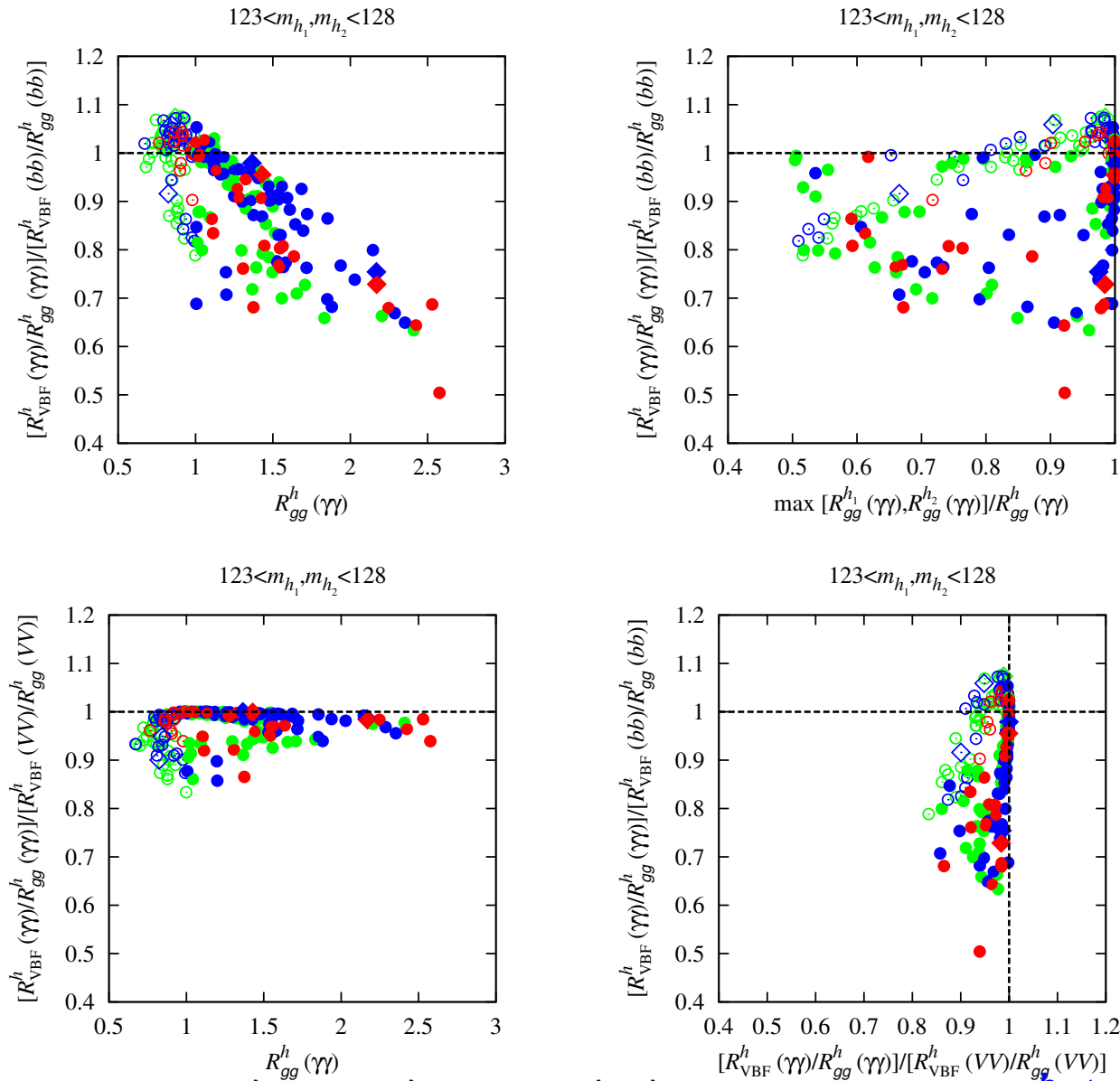


Figure 14: Double ratios I) and II) of Eq. (10) as functions of $R_{gg}^h(\gamma\gamma)$ (on the left). On the right we show (top) double ratio I) vs. $\max [R_{gg}^{h1}(\gamma\gamma), R_{gg}^{h2}(\gamma\gamma)] / R_{gg}^h(\gamma\gamma)$ and (bottom) double ratio I) vs. double ratio II) for the points displayed in Fig. 16. Colors and symbols are the same as in Fig. 16.

- What does current LHC data say about these various double ratios?

The central values and 1σ error bars for the numerator and denominator of double ratios I) and II) obtained from CMS data (CMS-PAS-HIG-12-020) are also shown in Fig. 16.

Obviously, current statistics are inadequate to discriminate whether or not the double ratios deviate from unity.

About 100 times increased statistics will be needed. This will not be achieved until the $\sqrt{s} = 14$ TeV run with $\geq 100 \text{ fb}^{-1}$ of accumulated luminosity.

Nonetheless, it is clear that the double-ratio diagnostic tools will ultimately prove viable and perhaps crucial for determining if the ~ 125 GeV Higgs signal is really only due to a single Higgs-like resonance or if two resonances are contributing.

Degeneracy has significant probability in model contexts if enhanced $\gamma\gamma$ rates are indeed confirmed at higher statistics.

Higgs at 125 GeV for LHC and 136 GeV for the Tevatron (and LHC?):

(G. Belanger, U. Ellwanger, J. F. Gunion, Y. Jiang and S. Kraml. arXiv:1208.4952)

- Need to reexamine in light of HCP data.
- However, some salient points that appear to remain relevant are the following:
 1. There is a clear signal for an H_1 at ~ 125 GeV.
 2. CMS may have an H_2 at ~ 136 GeV in the $\gamma\gamma$ final state.
ATLAS so far does not see a corresponding $\gamma\gamma$ peak.
 3. If $R_{VBF}^1(\tau\tau)$ at CMS and ATLAS remains somewhat suppressed while $R_{VH}(b\bar{b})$ measured at the Tevatron remains enhanced over a broad $M_{b\bar{b}}$ mass range and above what can come from the H_1 , then an H_2 with $M_{H_2} \sim 135\text{--}136$ GeV could provide the source of the extra $b\bar{b}$ events.
This possibility is one of the main advantages of this 125+136 idea.

4. Of course, the H_2 should not appear in the ZZ^* final state with much strength, since neither CMS nor ATLAS sees a 4ℓ mass peak near 136 GeV.

(CMS appears to have something at ~ 144 GeV, but ATLAS has only fluctuations in the relevant mass region.)

- The NMSSM is flexible enough to easily give a relevant scenario, but the precise model proposed in our original paper will need some adjustment.

And, of course, ATLAS would eventually need to see some signal in the $\gamma\gamma$ final state at 135 GeV.

Higgses at 98 GeV for LEP and 125 GeV for LHC:

(G. Belanger, U. Ellwanger, J. F. Gunion, Y. Jiang, S. Kraml and J. H. Schwarz.

arXiv:1210.1976)

- We demonstrate that the two lightest CP-even Higgs bosons, h_1 and h_2 , of the NMSSM could have properties such that the h_1 fits the LEP excess at ~ 98 GeV while the h_2 is reasonably consistent with the Higgs-like LHC signals at ~ 125 GeV, including in particular the larger-than-SM signal in the $\gamma\gamma$ channel.

To describe the LEP and LHC data the h_1 must be largely singlet and the h_2 primarily doublet (mainly H_u for the scenarios we consider).

An h_2 with $m_{h_2} \sim 125$ GeV and enhanced $\gamma\gamma$ rate is obtained, as in previous cases, at large λ and moderate $\tan\beta$.

- In order to display the ability of the NMSSM to simultaneously explain the LEP and LHC Higgs-like signals, we (once again) turn to NMSSM scenarios with semi-unified GUT scale soft-SUSY-breaking.

- All the accepted points correspond to scenarios that obey all experimental constraints (mass limits and flavor constraints as implemented in NMSSMTools, $\Omega h^2 < 0.136$ and 2011 XENON100 constraints on the spin-independent scattering cross section) except that the SUSY contribution to the anomalous magnetic moment of the muon, δa_μ , is too small to explain the discrepancy between the observed value of a_μ and the SM prediction.
- Fig. 15, the crucial plot, shows $R_{VBF}^{h_1}(bb)$ (which = $R_{Z^* \rightarrow Zh_1}^{h_1}(bb)$ as for LEP) versus $R_{gg}^{h_2}(\gamma\gamma)$ when $m_{h_1} \in [96, 100]$ GeV and $m_{h_2} \in [123, 128]$ GeV are imposed in addition to the above mentioned experimental constraints.¹

(In this and all subsequent plots, points with $\Omega h^2 < 0.094$ are represented by blue circles and points with $\Omega h^2 \in [0.094, 0.136]$ (the "WMAP window") are represented by orange diamonds.)

Note that $R_{VBF}^{h_1}(bb)$ values are required to be smaller than 0.3 by virtue of the fact that the LEP constraint on the $e^+e^- \rightarrow Zb\bar{b}$ channel with $M_{b\bar{b}} \sim 98$ GeV is included in the NMSSMTools program.

¹Here the Higgs mass windows are designed to allow for theoretical errors in the computation of the Higgs masses.

Those points with $R_{VBF}^{h_1}(bb)$ between about 0.1 and 0.25 would provide the best fit to the LEP excess.

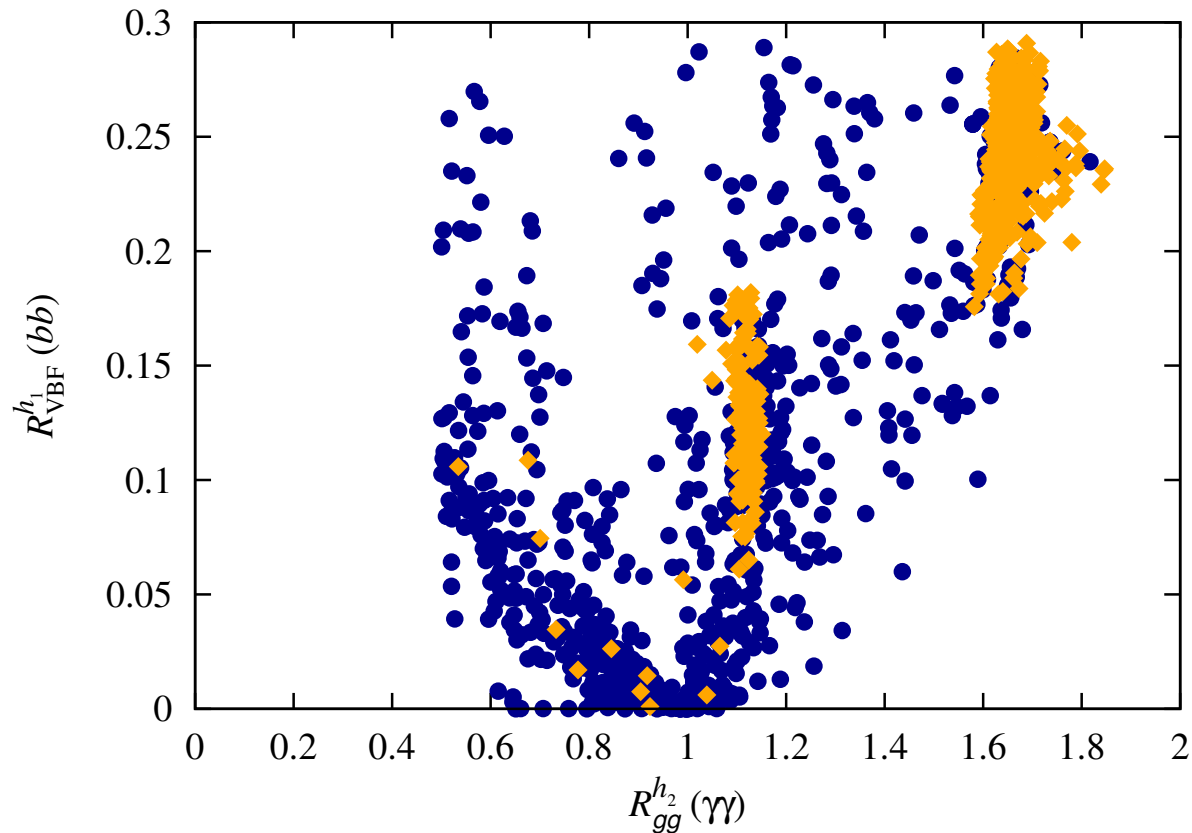


Figure 15: Signal strengths (relative to SM) $R_{VBF}^{h_1}(bb)$ versus $R_{gg}^{h_2}(\gamma\gamma)$ for $m_{h_1} \in [96, 100]$ GeV and $m_{h_2} \in [123, 128]$ GeV. In this and all subsequent plots, points with $\Omega h^2 < 0.094$ are represented by blue circles and points with $\Omega h^2 \in [0.094, 0.136]$ (the "WMAP window") are represented by orange diamonds.

In all the remaining plots we will impose the additional requirements: $R_{gg}^{h_2}(\gamma\gamma) > 1$ (for LHC enhancement) and $0.1 \leq R_{VBF}^{h_1}(bb) \leq 0.25$ (for LEP fit).

In the following, we will refer to these NMSSM scenarios as the “98 + 125 GeV Higgs scenarios” or “LEP-LHC scenarios”.

- Fig. 16 gives the essential results.

The upper plots show that the h_2 can easily have an enhanced $\gamma\gamma$ signal for both gg and VBF production whereas the $\gamma\gamma$ signal arising from the h_1 for both production mechanisms is quite small and unlikely to be observable.

Note the two different $R_{gg}^{h_2}(\gamma\gamma)$ regions with orange diamonds (for which Ωh^2 lies in the WMAP window), one with $R_{gg}^{h_2}(\gamma\gamma) \sim 1.1$ and the other with $R_{gg}^{h_2}(\gamma\gamma) \sim 1.6$. These same 2 regions emerge in many later figures.

The first region corresponds to $m_{\tilde{\chi}_1^0} > 93$ GeV and $m_{\tilde{t}_1} > 1.8$ TeV while the second region corresponds to $m_{\tilde{\chi}_1^0} \sim 77$ GeV and $m_{\tilde{t}_1}$ between 197 GeV and 1 TeV. If $R_{gg}^{h_2}(\gamma\gamma)$ ends up converging to a large value, then masses for all strongly interacting SUSY particles would be close to current limits.

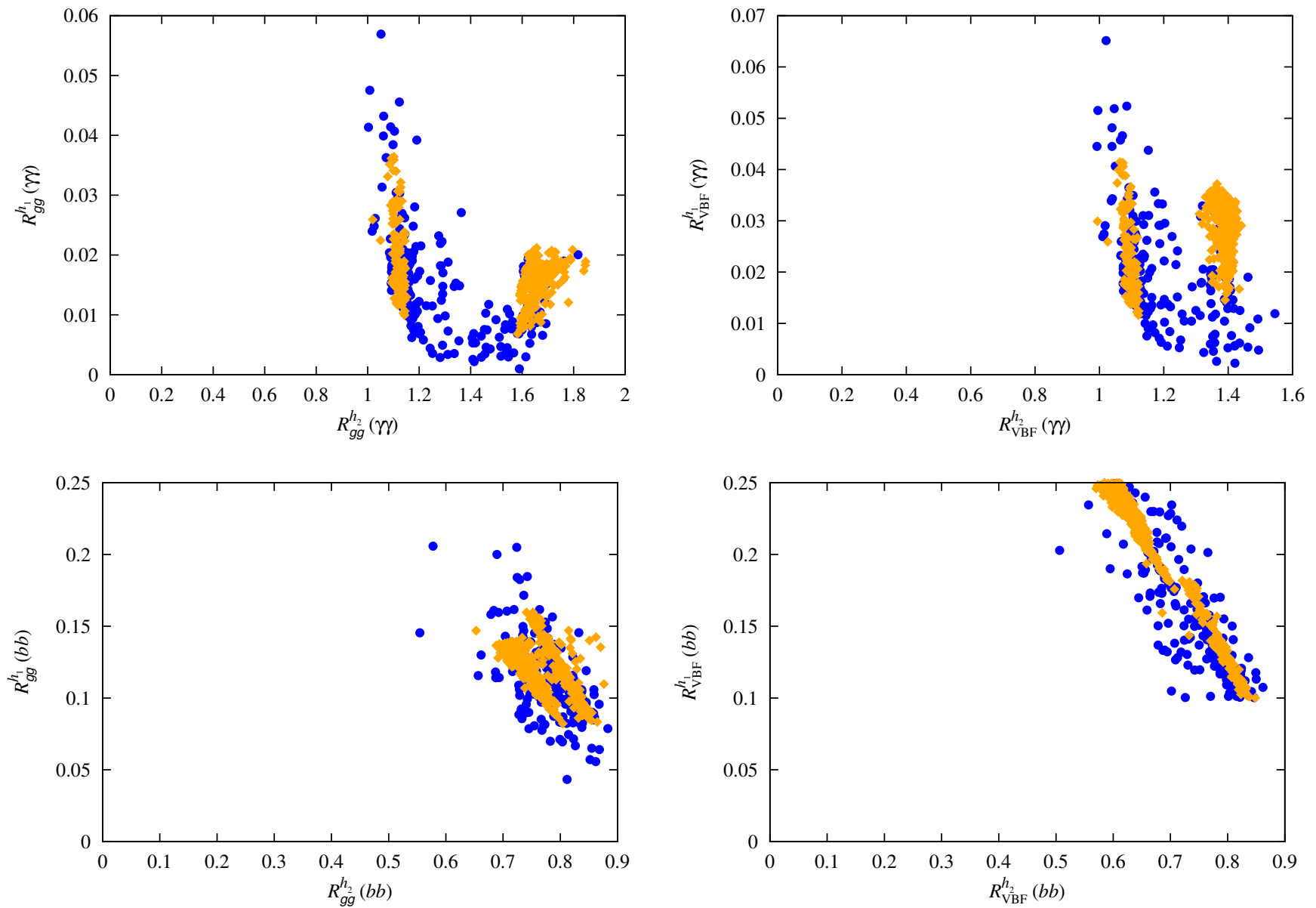


Figure 16: For $h = h_1$ and $h = h_2$, we plot (top) $R_{gg}^h(\gamma\gamma)$ and $R_{VBF}^h(\gamma\gamma)$ and (bottom) $R_{gg}^h(bb)$ and $R_{VBF}^h(bb)$ we show only points satisfying all the basic constraints as well as $m_{h_1} \in [96, 100]$ GeV, $m_{h_2} \in [123, 128]$ GeV, $R_{gg}^{h_2}(\gamma\gamma) > 1$ and $R_{VBF}^{h_1}(bb) \in [0.1, 0.25]$, *i.e.* the “98 + 125 GeV Higgs scenarios”.

- The **bottom row** of the figure focuses on the $b\bar{b}$ final state. We observe the reduced $R_{gg}^{h_2}(bb)$ and $R_{VBF}^{h_2}(bb)$ values associated with reduced $b\bar{b}$ width (relative to the SM) needed for enhanced $R_{gg}^{h_2}(\gamma\gamma)$ and $R_{VBF}^{h_2}(\gamma\gamma)$.

The $R_{gg}^{h_1}(bb)$ and $R_{VBF}^{h_1}(bb)$ values \Rightarrow the h_1 could not have been seen at the Tevatron nor (yet) at the LHC. Sensitivity to $R_{gg}^{h_1}(bb)$ ($R_{VBF}^{h_1}(bb)$) values from 0.05 to 0.2 (0.1 to 0.25) will be needed at the LHC.

This compares to expected sensitivities after the $\sqrt{s} = 8$ TeV run in these channels to R values of at best 0.8.²

Statistically, a factor of 4 to 10 improvement requires integrated luminosity of order 16 to 100 times the current $L = 10 \text{ fb}^{-1}$. Such large L values will only be achieved after the LHC is upgraded to 14 TeV.

Finally, note that for WMAP-window points the largest $R_{VBF}^{h_1}(bb)$ values occur for the light- $m_{\tilde{\chi}_1^0}$ point group described above for which supersymmetric particle masses are as small as possible.

²Here, we have used Fig. 12 of cmshiggs extrapolated to a Higgs mass near 98 GeV and assumed $L = 20 \text{ fb}^{-1}$ each for ATLAS and CMS.

- Other NMSSM particles, properties and parameters, including $\tilde{\chi}_1^0$ and $\tilde{\chi}_1^\pm$ compositions

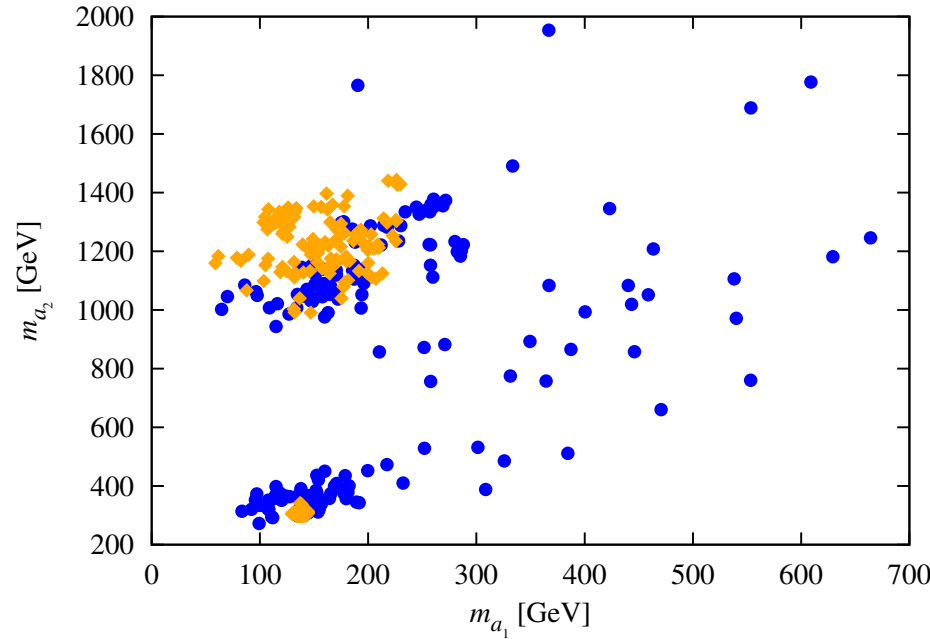


Figure 17: Scatter plot of m_{a_2} versus m_{a_1} for the 98+125 GeV scenario; note that $m_{a_2} \simeq m_{h_3} \simeq m_{H^\pm}$. Note that in this figure there is a dense region, located at $(m_{a_1}, m_{a_2}) \sim (130, 330)$ GeV, of strongly overlapping orange diamond points. These are the points associated with the low- $m_{\tilde{\chi}_1^0}$ WMAP-window region of parameter space. Corresponding dense regions appear in other figures.

We note without a plot that the good Ωh^2 points all have $m_{\tilde{\ell}_R}$, $m_{\tilde{\nu}_\ell}$, $m_{\tilde{\tau}_1}$ and $m_{\tilde{\nu}_\tau}$ larger than 1.5 TeV.

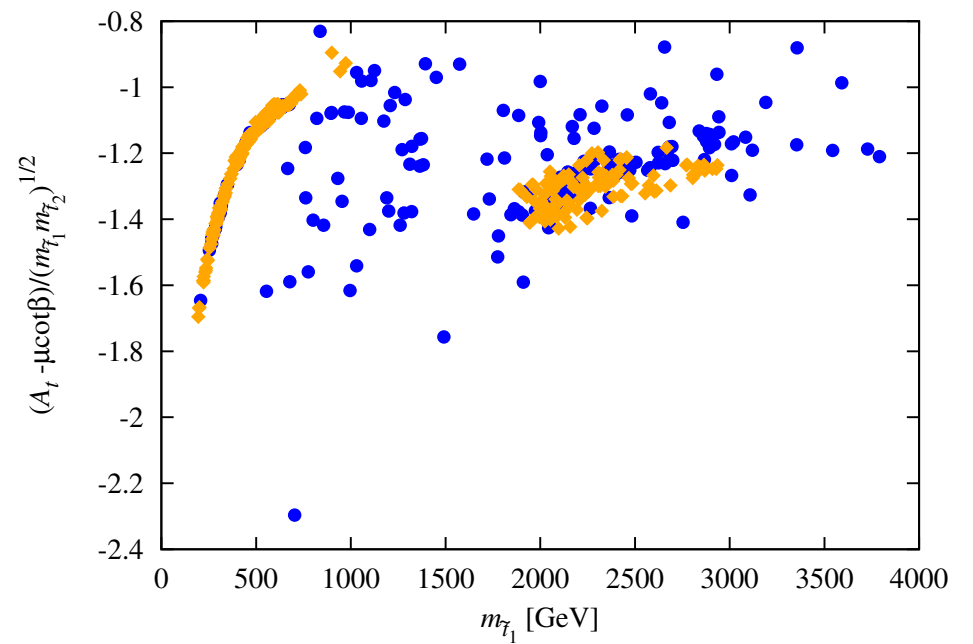
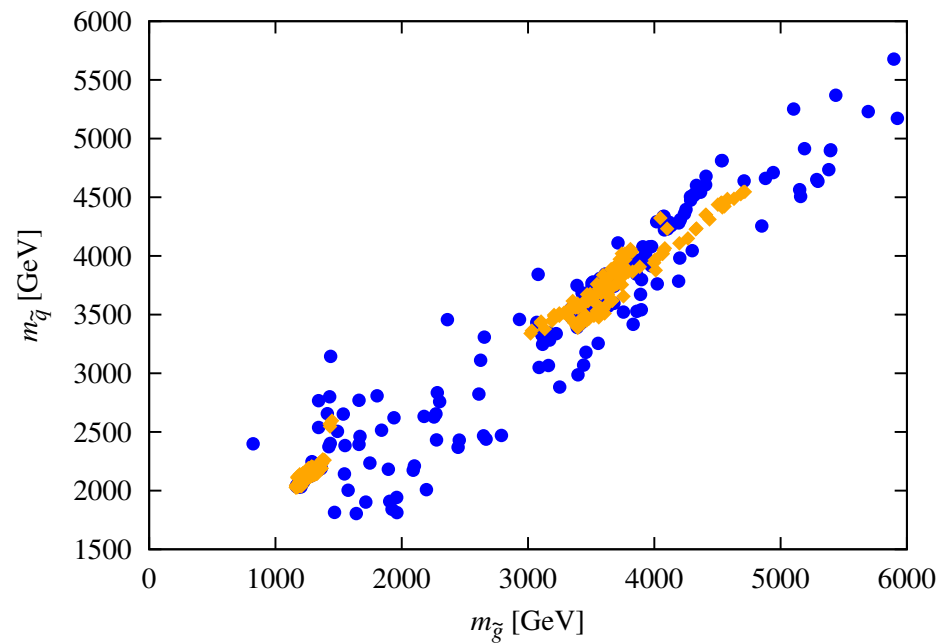
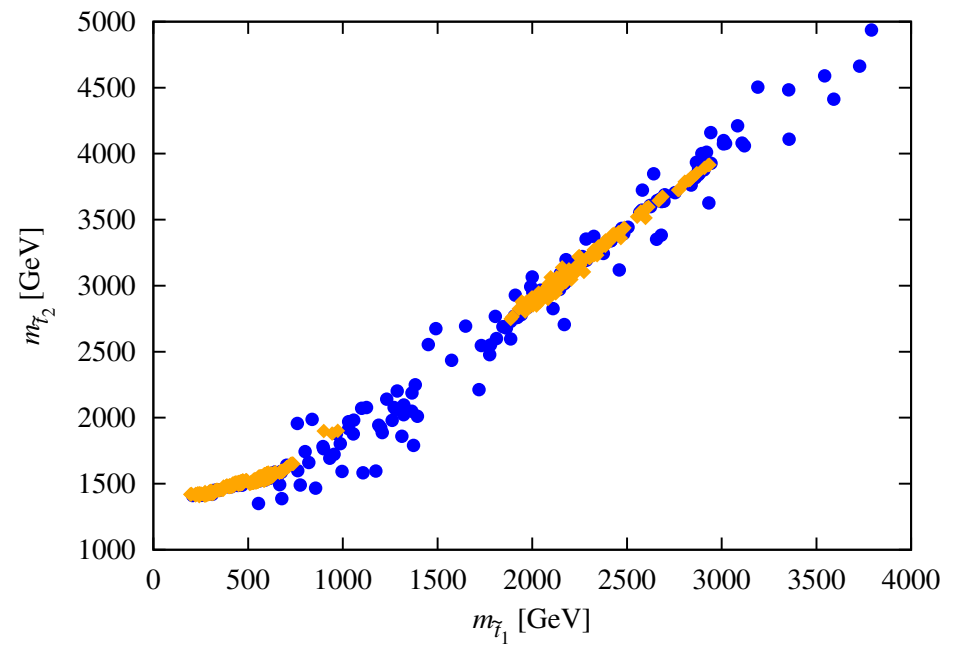
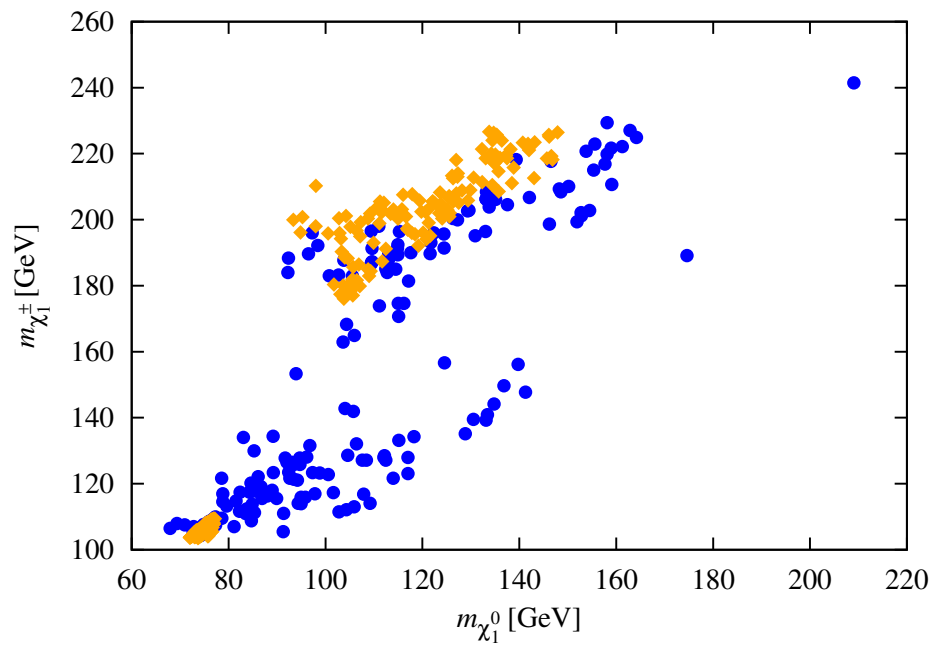


Figure 18: Plots showing $m_{\tilde{\chi}_1^0}$, $m_{\tilde{\chi}_1^\pm}$, $m_{\tilde{\tau}_1}$, $m_{\tilde{\tau}_2}$, $m_{\tilde{q}}$, $m_{\tilde{g}}$, and the mixing parameter $(A_t - \mu \cot \beta) / \sqrt{m_{\tilde{\tau}_1} m_{\tilde{\tau}_2}}$.

- **Input parameters** Note that the low- $m_{\tilde{\chi}_1^0}$ WMAP-window scenarios have not only low $m_{\tilde{t}_1}$ but also low μ_{eff} , implying not much fine-tuning.

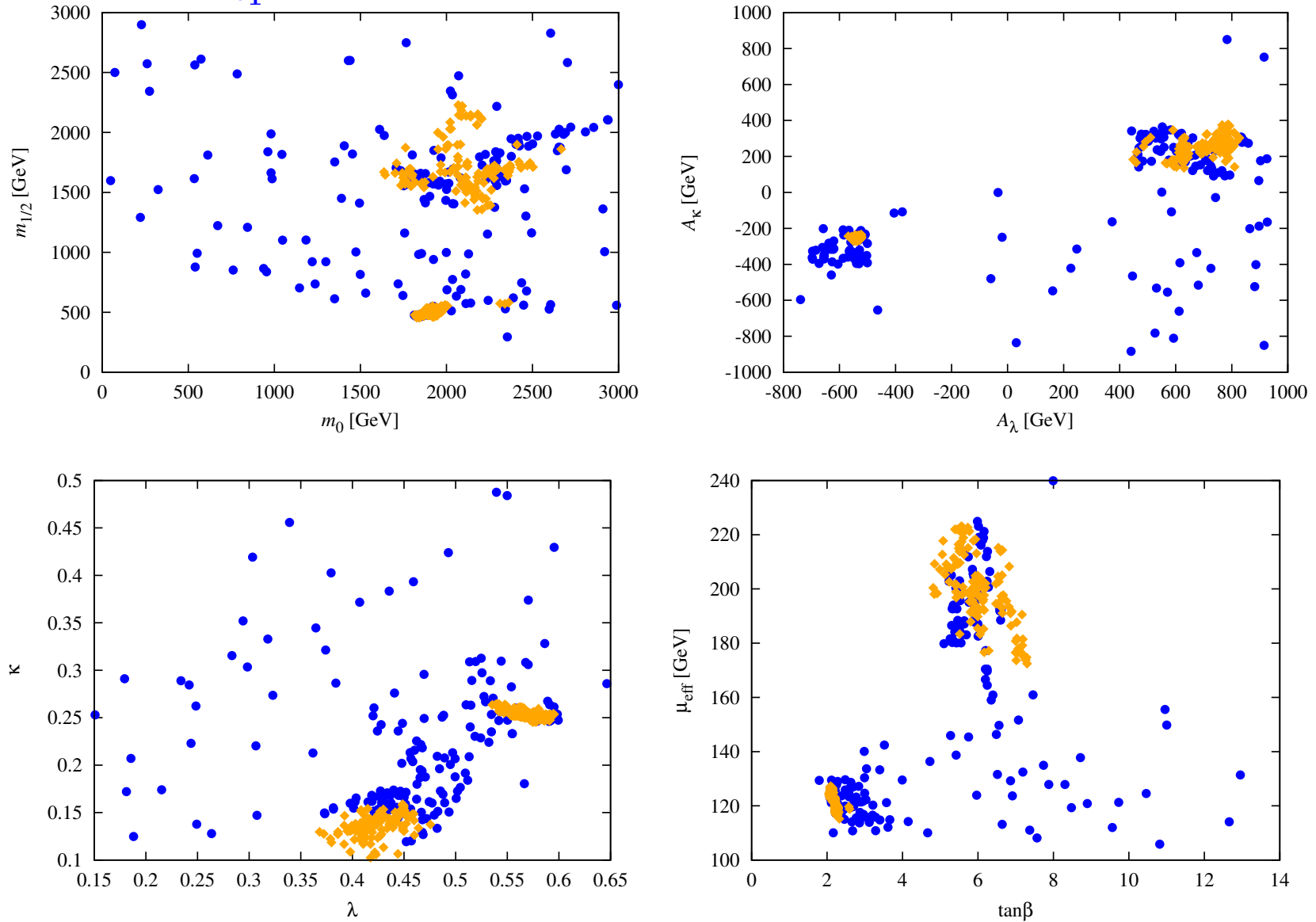


Figure 19: GUT scale and SUSY scale parameters leading to the LEP–LHC scenarios.

● Dark Matter Issues

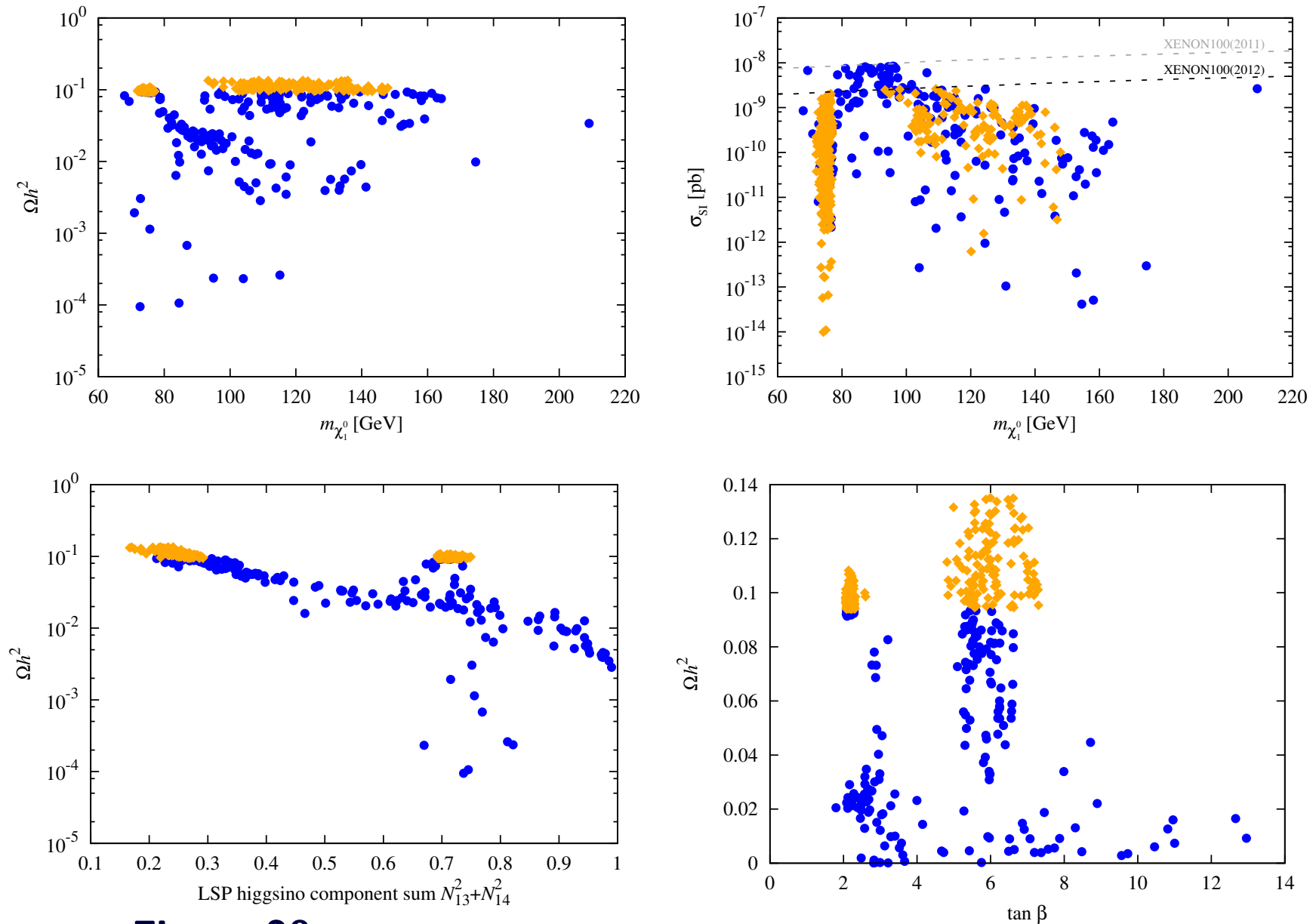


Figure 20: Dark matter properties for the LEP-LHC scenarios.

Dark matter (DM) properties for the surviving NMSSM parameter points are summarized in Fig. 20. Referring to the figure, we see a mixture of blue circle points (those with $\Omega h^2 < 0.094$) and orange diamond points (those with $0.094 \leq \Omega h^2 \leq 0.136$, *i.e.* in the WMAP window).

The main mechanism at work to make Ωh^2 too small for many points is rapid $\tilde{\chi}_1^0 \tilde{\chi}_1^0$ annihilation to $W^+ W^-$ due to a substantial higgsino component of the $\tilde{\chi}_1^0$ (see third plot of Fig. 20). Indeed, the relic density of a higgsino LSP is typically of order $\Omega h^2 \approx 10^{-3} - 10^{-2}$.

To avoid this, need $\tilde{\chi}_1^0 \tilde{\chi}_1^0 \rightarrow W^+ W^-$ below threshold as for the light $\tilde{\chi}_1^0$ point group (the strongly overlapping points with $m_{\tilde{\chi}_1^0} < m_W$)

As the higgsino component declines Ωh^2 increases it is the points for which the LSP is dominantly singlino that have large enough Ωh^2 to fall in the WMAP window. This kind of point appears in the large- $m_{\tilde{\chi}_1^0}$ point group.

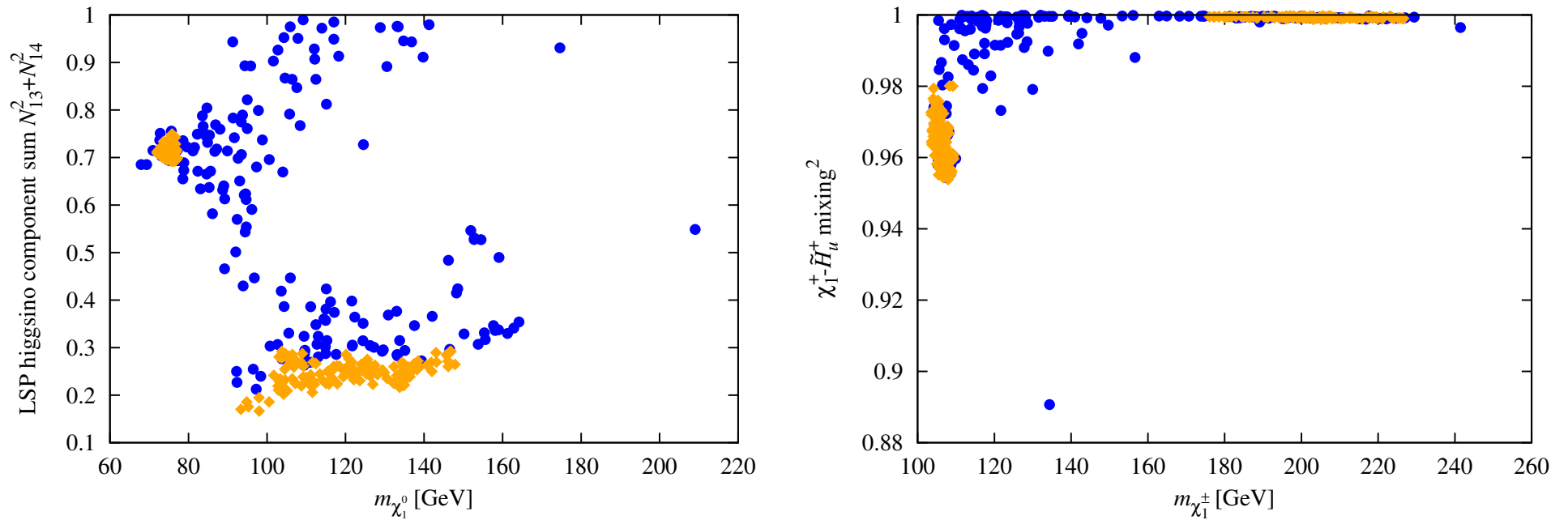


Figure 21: Neutralino and chargino compositions for the LEP–LHC scenarios.

Also plotted in Fig. 20 is the spin-independent direct detection cross section, σ_{SI} , as a function of $m_{\tilde{\chi}_1^0}$. Experiments will reach sensitivities that will probe some of the predicted σ_{SI} values relatively soon, especially the $m_{\tilde{\chi}_1^0} > 93$ GeV points that are in the WMAP window.

However, it is also noteworthy that the $m_{\tilde{\chi}_1^0} \sim 75$ GeV WMAP-window points can have very small σ_{SI} .

- Direct Higgs production and decay at the LHC

We have already noted in the discussion of Fig. 16 that gg and VBF production of the h_1 with $h_1 \rightarrow b\bar{b}$ provide event rates that might eventually be observable at the LHC once much higher integrated luminosity is attained. Other possibilities include production and decay of the a_1 , a_2 , and h_3 .

Since the a_1 is dominantly singlet in nature, its production rates at the LHC are rather small.

Since the a_2 and h_3 are dominantly doublet they provide better discovery prospects.

Decay branching ratios and LHC cross sections in the gg fusion mode for a_2 and h_3 are shown in Fig. 22.

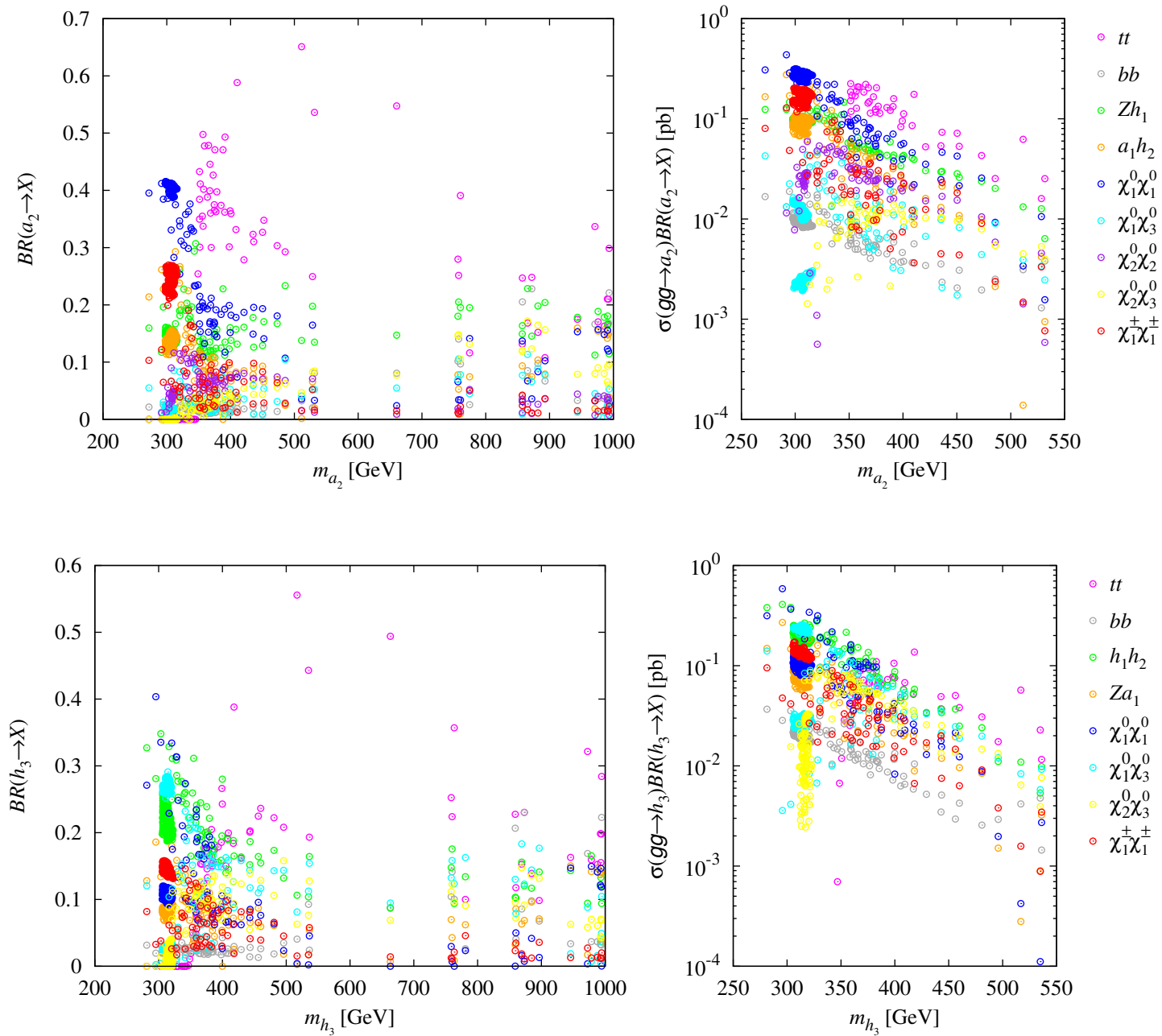


Figure 22: Decay branching ratios and LHC cross sections in the gg fusion mode (at $\sqrt{s} = 8$ TeV) for a_2 and h_3

- If $m_{a_2} > 2m_t$, the $t\bar{t}$ final state has $\sigma(gg \rightarrow a_2)\text{BR}(a_2 \rightarrow t\bar{t}) > 0.01$ pb for $m_{a_2} < 550$ GeV, implying > 200 events for $L = 20 \text{ fb}^{-1}$.

A study is needed to determine if this would be observable in the presence of the $t\bar{t}$ continuum background.

No doubt, efficient b tagging and reconstruction of the $t\bar{t}$ invariant mass in, say, the single lepton final state would be needed.

- For $m_{a_2} < 2m_t$, the $X = a_1 h_2$ final state with both a_1 and h_2 decaying to $b\bar{b}$ might be visible above backgrounds.

However, a dedicated study of this particular decay mode is still lacking.

Similar remarks apply in the case of the h_3 where the possibly visible final states are $t\bar{t}$ for $m_{h_3} > 2m_t$ and $h_1 h_2$ for $m_{h_3} < 2m_t$.

For both the a_2 and h_3 , $\sigma\text{BR}(X)$ is substantial for $X = \tilde{\chi}_1^0 \tilde{\chi}_1^0$, but to isolate this invisible final state would require an additional photon or jet tag which would reduce the cross section from the level shown.

Well, the story goes, with complicated decays of neutralinos and charginos to the various lighter Higgs bosons.

No time to go into it all here.

We do think this scenario is an intriguing one and hope experimentalists will educate themselves about some of its peculiarities.

It is possible, but far from guaranteed (in the low- $m_{\tilde{\chi}_1^0}$ region), that σ_{SI} is large enough to be detectable soon.

The pure 2HDM

- “Two-Higgs-Doublet Models and Enhanced Rates for a 125 GeV Higgs” A. Drozd, B. Grzadkowski, J. F. Gunion and Y. Jiang. arXiv:1211.3580 [hep-ph]
- see also, “Mass-degenerate Higgs bosons at 125 GeV in the Two-Higgs-Doublet Model” P. M. Ferreira, H. E. Haber, R. Santos and J. P. Silva. arXiv:1211.3131 [hep-ph]
- There are some differences.
- We employ the 2HDMC code.³ It implements:
 1. Precision electroweak constraints (denoted STU)
 2. Limits coming from requiring vacuum stability, unitarity and coupling-constant perturbativity (denoted jointly as SUP).

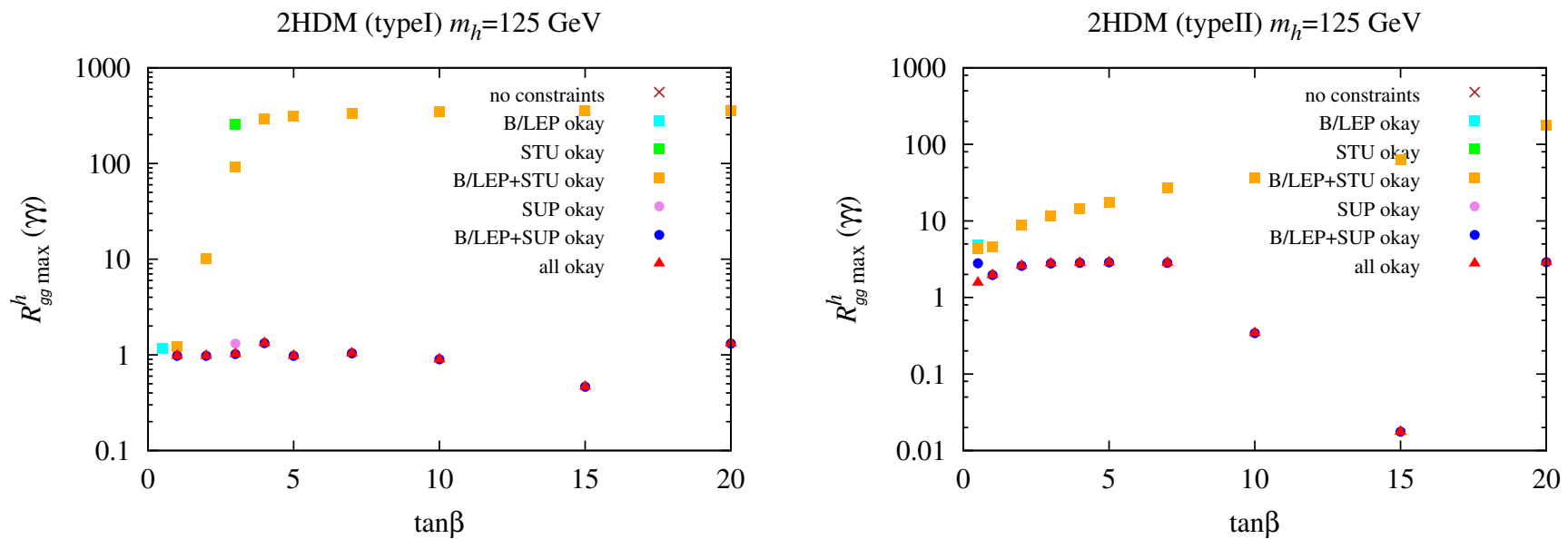
The SUP constraints are particularly crucial in limiting the level of enhancement of the $gg \rightarrow h \rightarrow \gamma\gamma$ channel, our main focus.
- For all our scans, we have supplemented the 2HDMC code by including the B/LEP constraints.
 1. For the LEP data we adopt upper limits on $\sigma(e^+e^- \rightarrow Z h/H)$ and $\sigma(e^+e^- \rightarrow A h/H)$ from Abbiendi:2002qp and Abbiendi:2004gn, respectively.

³We have modified the subroutine in 2HDMC that calculates the Higgs boson decays to $\gamma\gamma$ and also the part of the code relevant for QCD corrections to the $q\bar{q}$ final state.

2. Regarding B physics, the constraints imposed are those from $\text{BR}(B_s \rightarrow X_s \gamma)$, R_b , ΔM_{B_s} , ϵ_K , $\text{BR}(B^+ \rightarrow \tau^+ \nu_\tau)$ and $\text{BR}(B^+ \rightarrow D \tau^+ \nu_\tau)$.

The most important implications of these results are to place a lower bound on m_{H^\pm} as a function of $\tan \beta$ as shown in Fig. 15 of Branco:2011iw in the case of the Type II model and to place a lower bound on $\tan \beta$ as a function of m_{H^\pm} as shown in Fig. 18 of Branco:2011iw.

- We scan and find results illustrated by the following plot.



The top two plots show the maximum $R^h_{gg}(\gamma\gamma)$ values in the Type I (left) and Type II (right) models for $m_h = 125$ GeV as a function of $\tan \beta$ after imposing various constraints — see figure legend.

Disappearance of a point after imposing a given constraint set means that the point did not satisfy that set of constraints.

For boxes and circles, if a given point satisfies subsequent constraints then the resulting color is chosen according to the color ordering shown in the legend.

- Corresponding $R_{gg}^h(ZZ)$ and $R_{gg}^h(bb)$ are shown in Fig. 23.

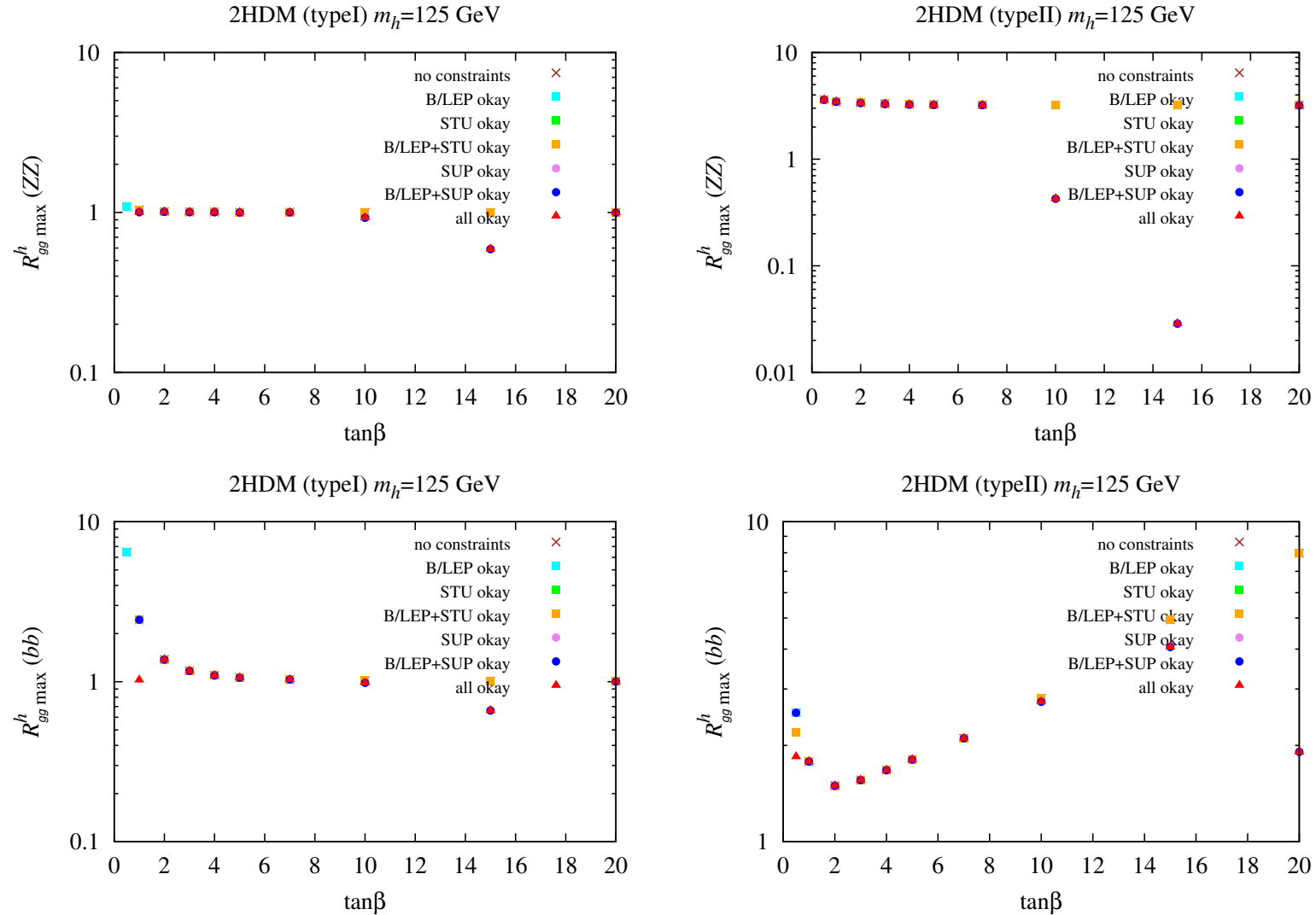


Figure 23: ZZ and $b\bar{b}$ final states for parameters with maximum $R_{gg}^h(\gamma\gamma)$.

Summary of results:

- Type II model:

1. For only h at 125 GeV, the parameters that give $R_{gg}^h(\gamma\gamma) > 1.3$ are characterized by $R_{gg}^h(ZZ) > R_{gg}^h(\gamma\gamma)$, a result that is inconsistent with experimental results in the $gg \rightarrow h \rightarrow ZZ \rightarrow 4\ell$ channel.

Thus, if $R_{gg}^h(\gamma\gamma) > 1.3$ and $R_{gg}^h(ZZ) < 1.3$ both persist experimentally, the Type II model cannot describe the data if only the h resides at 125 GeV.

2. Similar statements apply to the case of the heavier H having a mass of 125 GeV.
3. For approximately degenerate h and A Higgs bosons at 125 GeV there exist theoretically consistent parameter choices for Type II models for which $R_{gg}^{h+A}(\gamma\gamma) > 1.3$ while $R_{gg}^{h+A}(ZZ) < 1.3$, but in these cases $R_{gg}^{h+A}(b\bar{b}) > 3.75$, a value far above that observed.

Thus, the Type II 2HDMs cannot yield $R_{gg}^{h+A}(\gamma\gamma) > 1.3$ without conflicting with other observables.

In short, the Type II model is unable to give a significantly enhanced $gg \rightarrow h \rightarrow \gamma\gamma$ signal while maintaining consistency with other channels.

- Type I model:

1. The maximal $R_{gg}^h(\gamma\gamma)$ is of order of 1.3, as found if $\tan\beta = 4$ or 20.
2. In these cases, $R_{gg}^h(ZZ)$ and $R_{gg}^h(b\bar{b})$ are of order 1 as fairly consistent with current data.
3. For these scenarios, the charged Higgs is light, $m_{H^\pm} = 90$ GeV.
4. Despite this small mass, there is no conflict with LHC data due to the fact that

$BR(t \rightarrow H^+ b) \sim 1/\tan^2 \beta$ is small enough to be below current limits.

Thus, Type I models could provide a consistent picture if the LHC results converge to only a modest enhancement for $R_{gg}^h(\gamma\gamma) \lesssim 1.3$.

But, if $R_{gg}^h(\gamma\gamma)$ is definitively measured to have a value much above 1.3 while the ZZ and $b\bar{b}$ channels show little enhancement then there is no consistent 2HDM description.

- Perhaps the pure 2HDM is too limiting and one must go beyond the 2HDM to include new physics such as supersymmetry.

Conclusions

- It seems likely that the Higgs responsible for EWSB has emerged.
- Perhaps, other Higgs-like objects are emerging.
- Survival of enhanced signals for one or more Higgs boson would be one of the most exciting outcomes of the current LHC run and would guarantee years of theoretical and experimental exploration of BSM models with elementary scalars.
- $>$ SM signals would appear to guarantee the importance of a linear collider or LEP3 or muon collider in order to understand fully the responsible BSM physics.
- In any case, the current situation illustrates the fact that we must never assume we have uncovered all the Higgs.

Certainly, I will continue watching and waiting

